# The glycan hole area of HIV-1 envelope trimers contributes prominently to the induction of autologous neutralization

Anna Schorcht[1], Christopher A. Cottrell[2], Pavel Pugach[3,a], Rajesh P. Ringe[3], Alvin X. Han[4], Joel D. Allen[5], Tom L.G.M. van den Kerkhof[1,6,b], Gemma E. Seabright[5], Edith E. Schermer[1], Thomas J. Ketas[3], Judith A. Burger[1], Jelle van Schooten[1], Celia C. LaBranche[7], Gabriel Ozorowski[2], Natalia de Val[2,c], Daniel L.V. Bader[2], Hanneke Schuitemaker[6,b], Colin A. Russell[4], David C. Montefiori[7], Marit J. van Gils[1], Max Crispin[5], P.J. Klasse[3], Andrew B. Ward[2], John P. Moore[3], Rogier W. Sanders[1,3,*]

[1]Department of Medical Microbiology and Infection Prevention, Amsterdam Infection & Immunity Institute (AI&AII), Amsterdam UMC, Location Meibergdreef, University of Amsterdam, Amsterdam, The Netherlands

[2]Department of Integrative Structural and Computational Biology, The Scripps Research Institute, La Jolla, California, USA

[3]Department of Microbiology and Immunology, Weill Cornell Medical College, New York, New York, USA

[4]Laboratory of Applied Evolutionary Biology, Department of Medical Microbiology and Infection Prevention, Amsterdam Infection & Immunity Institute (AI&AII), Amsterdam UMC, Location Meibergdreef, University of Amsterdam, Amsterdam, The Netherlands

[5]Centre for Biological Sciences and Institute for Life Sciences, University of Southampton, Southampton, England, United Kingdom

[6]Department of Experimental Immunology, Amsterdam Infection & Immunity Institute (AI&AII), Amsterdam UMC, Location Meibergdreef, University of Amsterdam, Amsterdam, The Netherlands

[7]Department of Surgery, Duke University Medical Center, Durham, North Carolina, USA

[a] Current Address: Applied Biological Labs, Brooklyn, New York, USA

[b] Current Address: Janssen Vaccines & Prevention, Leiden, The Netherlands

[c] Current Address: Thermo Fisher Scientific, Frederick, Maryland, USA

*Corresponding author: Rogier W. Sanders, r.w.sanders@amsterdamumc.nl

## Abstract

The HIV-1 envelope glycoprotein trimer (Env) is heavily glycosylated, creating a dense glycan shield that protects the underlying peptidic surface from antibody recognition. The absence of conserved glycans, due to missing potential N-linked glycosylation sites (PNGS), can result in strain-specific, autologous neutralizing antibody (NAb) responses. Here we sought to gain a deeper understanding of the autologous neutralization by introducing holes in the otherwise dense glycan shields of the AMC011 and AMC016 SOSIP trimers. Specifically, when we knocked out the N130 and N289 glycans, which are absent from the well-characterized B41 SOSIP trimer, we observed stronger autologous NAb responses. We also analyzed the highly variable NAb responses induced in rabbits by diverse SOSIP trimers from subtypes A, B and C. Statistical analysis, using a linear regression analysis, revealed that the cumulative area exposed on a trimer by glycan holes correlates with the magnitude of the autologous NAb response.


## Importance

40 years after the first description of HIV-1 the search for a protective vaccine is still ongoing. The sole target for antibodies that can neutralize the virus are the trimeric envelope glycoproteins (Env) located on the viral surface. The glycoprotein surface is covered with glycans that shield off the underlying protein components from recognition by the immune system. However, the Env trimers of some viral strains have holes in the glycan shield. Immunized animals developed antibodies against such glycan holes. These antibodies are generally strain-specific. Here we sought to gain a deeper understanding of what drives these specific immune responses. First, we show that strain-specific neutralizing antibody responses can be increased by creating artificial holes in the glycan shield. Second, when studying a diverse set of Env trimers with different characteristics, we found that the surface area of the glycan holes contributes prominently to the induction of strain-specific neutralizing antibodies.

## Introduction

The human immunodeficiency virus type 1 (HIV-1) envelope glycoprotein (Env) is located on the surface of virus particles, and is the target of neutralizing antibodies (NAbs), that are produced during infection. Accordingly, the Env trimer is central to vaccine development strategies aimed at inducing NAbs (1). The assembled Env trimer consists of three heterodimers, each formed by a gp41 and gp120 subunit. Vaccines based on Env, such as native-like SOSIP trimers, induced autologous and, sporadically, heterologous tier 2 NAbs in animals (2–5). Two major complications to the induction of potent and consistent neutralization breadth are the extreme diversity of HIV-1 Env and its extensive glycosylation (6–8). The trimer contains around 90 potential N-linked glycosylation sites (PNGS), which account for approximately half of the molecular mass of the external domains of the Env trimer (9). Differences in the number and precise locations of these glycans contribute to the overall variation in Env proteins. During trimer synthesis in the endoplasmic reticulum (ER), N-linked glycans can be attached to a PNGS that is defined by the motifs asparagine-x-threonine (NxT) or asparagine-x-serine (NxS), where x can be any amino acid except proline (10, 11). Glycans are attached to Env as oligomannose-type glycans, some of which are further processed in the Golgi compartment while others remain under-processed, particularly ones that form a cluster on the gp120 outer domain and that are located at the trimer apex (12–15).

The densely packed glycans on the trimer surface shield the underlying peptidic surface from recognition by the immune system. Nevertheless, the glycan shield is not impenetrable. First, although N-linked glycans are host cell-derived and generally poorly immunogenic, they can contribute to multiple protein/glycan composite epitopes for broadly neutralizing antibodies (bNAbs) (7, 16). Second, the glycan shields often have holes created by the absence of one or more PNGS that are typically well conserved (i.e., present in > 50% of HIV-1 group M strains). Glycan holes tend to be immunogenic and can induce strain-specific, autologous NAb responses (4, 17–19). Thus, knocking-out selected glycans on Env trimers increases the autologous NAb response, which is directed to the newly created holes (19, 20). As HIV-1 isolates with a complete glycan shield on Env might induce bNAbs more readily than ones with holes, glycan-dense trimers have been designed accordingly (3, 21–23).

To date, studies on how glycan holes influence SOSIP trimer immunogenicity have involved only trimers from a few genotypes. In this study we sought to increase our understanding of this relationship by introducing artificial holes in the naturally dense glycan

shields on trimers from the subtype B strains AMC011 and AMC016. In addition, we analyzed how well a large panel of SOSIP trimers with different glycan shield characteristics could induce autologous NAbs. Factors that could contribute to the induction of autologous NAbs were defined and assessed with a linear regression analysis. This analysis pointed at glycan hole area as a major driver for the induction of autologous NAb responses. Since multiple SOSIP trimers are moving into clinical phase testing (24), it is important to increase our understanding of the relationship between glycan holes and autologous NAb responses. Defining immunodominant glycan holes on Env trimers could facilitate the re-design of these trimers, as holes can be opened or closed as desired (19).

## Results

### The deletion of conserved PNGS alters the glycan shield of AMC011 and AMC016 trimers

To assess the impact on autologous neutralization when glycan holes are introduced into an otherwise complete glycan shield, we worked with two subtype B SOSIP trimers. The AMC011 SOSIP trimer, derived from a participant of the Amsterdam Cohort Studies (ACS), has a complete glycan shield; i.e., all the conserved PNGS, defined as present in >50% of HIV-1 group M viruses, are present in the AMC011 sequence (3). We have previously reported that AMC011 SOSIP trimers induced autologous NAbs weakly and inconsistently in immunized rabbits (3). The second subtype B trimer, AMC016 SOSIP, which has not been previously described, also has an apparently complete glycan shield as defined by the presence of all conserved PNGS.

The AMC016 *env* sequence was obtained 7-month post-seroconversion from an ACS-participant that did not develop bNAbs. Stabilizing mutations were introduced to the gp140 sequence, to create AMC016 SOSIP.v4.2 (2). The PGT145-purified protein was analyzed with negative-stain electron microscopy (NS-EM) and differential scanning calorimetry (DSC). The protein had a native-like trimer morphology (100%) and its midpoint of thermal denaturation ($T_m$) was 63°C (Fig. 1A and Table 1). The AMC016 trimer structure was solved by cryo-EM and is presented below.

To get a better understanding of the glycans present on the AMC016 SOSIP.v4.2 trimer, we first analyzed the overall glycan composition, using hydrophilic interaction chromatography-ultra-performance liquid chromatography (HILIC-UPLC) (Fig. 1B and Table 1). The majority of glycans are oligomannose-type (53.4% are $Man_{5-9}$), nearly half of which (23.9%) are $Man_9GlcNac_2$ (hereafter referred to as $Man_9$). For comparison, the AMC011 SOSIP.v5.2 trimer has a slightly higher proportion of oligomannose-type glycans (58.2%), whereas the $Man_9$ content was nearly the same (23.0%) (3).

Second, the site-specific glycan composition and occupancy of all 29 conserved PNGS on the AMC016 trimer were assessed by liquid chromatography-mass spectrometry (LC-MS). Most of the PNGS are dominated by oligomannose glycans (Fig. 1C, green), but the N136, N142, N462 and N625 sites contain predominantly complex glycans (Fig. 1C, pink). The high number of oligomannose glycans might reflect how a dense glycan shield restricts mannosidase access to individual sites (16). The majority of PNGS are fully occupied, or almost so (>90%), but there is lower occupancy of the N130, N134b, N142, N241, N289,

N301, N611 and N616 sites (67%, 72%, 58%, 79%, 52%, 87%, 37% and 17% occupied, respectively) (Fig. 1C, grey). Overall, the AMC011 and AMC016 SOSIP trimers were similar in respect of the number and location of PNGS (3). Thus, on the AMC011 trimer, the PNGS are mostly occupied by oligomannose glycans, but with mostly complex glycans at the N88, N141c, N355, N461 and N625 sites (3). The N141, N241, N611, N616 and N637 sites are <90% occupied (22%, 86%, 8%, 3% and 85% occupied, respectively). The composition and occupancy of N289, N392 and N396 glycans on the AMC011 trimer could not be resolved (3).

The two subtype B trimers, AMC011 and AMC016, have a complete glycan shield, as judged by the presence of all conserved PNGS, and hence are suitable for studying the impact of glycan holes on autologous neutralization. When designing the holes in the glycan shields, we used the subtype B B41 SOSIP trimer as a frame of reference for the PNGS we deleted. This trimer lacks two conserved glycans: N130 and N289 (18, 25). Rabbits immunized with B41 SOSIP trimers developed strong NAb responses against the autologous virus that were directed against the N289 glycan hole, a finding confirmed by the cloning of monoclonal antibodies (18, 26). The N130 glycan hole, located at the trimer apex, was reported to have no or only a minor effect on the induction of autologous NAbs (18). We knocked out both the conserved PNGS at N130 and N289 to create the Δ130Δ289 trimers (Fig. 2A). The goal was to see whether the new holes would be immunogenic for autologous NAbs in the context of the AMC011 and AMC016 SOSIP trimers. In both cases, we mimicked the amino acid composition at the bottom of the corresponding holes on the B41 trimer. Thus, the NCT motif at N130 was altered to NCN and the next two residues, DL, were changed to their B41 counterparts, NV (i.e., NCTDL to NCNNV). Similarly, the PNGS at N289 were changed from NKS to NEA for AMC011 SOSIP and NES to NEA for AMC016 SOSIP.

The resulting AMC011 and AMC016 SOSIP Δ130Δ289 trimers were expressed, affinity-purified using PGT145 and characterized. The purified proteins were trimers (Fig. 2B, BN-PAGE) that were fully cleaved between gp120 and gp41 (Fig. 2B, SDS-PAGE). The yields were slightly lower than for the parental trimer (1.0 mg/L *versus* 2.1 mg/L and 1.5 mg/L *versus* 2.0 mg/L for the AMC011 and AMC016 trimers, respectively) (Table 1). NS-EM showed that both trimers were predominantly, although not completely, in a native-like structure (88% for AMC011 SOSIP Δ130Δ289 and 78% for AMC016 SOSIP Δ130Δ289) (Fig. 2C and Table 1). These levels were lower than seen with the parental AMC011 and AMC016 SOSIP trimers, which had fully native like structures (100% in both cases) (Table 1) (3). In a DSC analysis, the $T_m$ values for the AMC011 parental and

Δ130Δ289 trimers were 67°C and 64°C, respectively, while the corresponding values for the AMC016 parental and Δ130Δ289 trimers were both 63°C (Table 1). The glycan-deleted AMC011 and AMC016 trimers had similar antigenicity profiles to the corresponding parental trimers when probed in an enzyme-linked immunosorbent assay (ELISA) using a panel of bNAbs and the non-neutralizing antibody, 17b, with and without soluble CD4 (Fig. 2D).

We used the HILIC-UPLC method to study how the glycan deletions affected the overall composition of the glycan shield, and to compare the mutant trimers with their parental counterpart. Knocking-out the N130 and N289 sites slightly decreased the oligomannose glycan content of the AMC011 trimer (58.2% for parental *versus* 50% for the glycan mutant) (Fig. 2E and Table 1) (3). The largest decrease was observed for $Man_9$ (23% *versus* 16.5%). Deleting both glycans had the opposite effect on the AMC016 trimer in that the oligomannose glycan content slightly increased (53.4% for parental *versus* to 57.6% for the glycan mutant), the largest increase was again for $Man_9$ (23.9% *versus* 26.4%) (Fig. 2E and Table 1).

The mutant trimers were also studied by LC-MS to obtain information on the site-specific glycan composition and occupancy. The majority of the 28 PNGS analyzed on the AMC011 Δ130Δ289 trimer were oligomannose-type glycans (Fig. 3A). However, the N88, N141, N141C, N188, N355, N461, N611 and N625 sites had >50% processed, complex-type glycans. Most of the PNGS were fully occupied; sites that were occupied to < 90% were N136, N141, N611, N616 and N637 (79%, 80%, 60%, 1% and 78%, respectively). Similarly, the 29 PNGS on the AMC016 Δ130Δ289 trimer were mostly occupied by oligomannose-type glycans, although >50% of the glycans on the N356 and N462 sites were complex (Fig. 3B). Again, PNGS occupancy was high, with the exception of N142, N611 and N616 (59%, 29% and 22% occupied, respectively).

A comparison of the glycan mutants with the corresponding parental trimers showed that knocking-out the N130 and N289 glycans altered the $Man_9$ content at a few specific PNGS (Fig. 4). The percentage point (pp) difference was calculated (% $Man_9$ mutant trimer - % $Man_9$ parental trimer) for sites where $Man_9$ was resolved (see Fig. 3) (16). For AMC011 Δ130Δ289, the glycan knock-out resulted in a substantial decrease in $Man_9$ at the N339 site (75 pp decrease; Fig. 4, yellow), which is adjacent to where the N289 glycan would be located. This outcome is consistent with previous observations that knocking-out one glycan site can increase mannosidase access to nearby glycans, but not more distant ones (16). In the case of the AMC016 Δ130Δ289 trimer, the glycan knock-out also decreased the $Man_9$ content of N339 (32 pp drop; Fig. 4, lilac). In addition, the $Man_9$ content decreased at sites N156,

N160 and N197 (32, 27 and 19 pp decrease, respectively), which are located on the trimer apex and in close proximity to the N130 glycan hole.

Knocking-out the N130 and N289 glycans had moderate impact on PNGS occupancy (see Fig. 1C and Fig. 3). Thus, N141 and N611 occupancy on the AMC011 Δ130Δ289 trimer increased for by 58 and 52 pp, respectively, reaching 80% and 60%. In contrast, occupancy decreased for N136 by 21 pp, reaching 79%. For the AMC016 Δ130Δ289, N134b, N241 and N301 occupancy increased by 28, 20 and 13 pp, respectively, reaching 99-100%.

In summary, we produced two stable, native-like Δ130Δ289 trimers based on the subtype B isolates AMC011 and AMC016. Both mutant trimers have comparable biophysical and biochemical properties to their parental counterpart, although the percentages in native-like form were slightly reduced. Knocking-out the N130 and N289 PNGS had a localized impact on the composition and occupancy of a few neighboring glycans, but only subtle effects elsewhere. The mutant trimers resemble the B41 SOSIP trimer in respect of the number and position of holes in their glycan shields, which are otherwise complete.

**The introduction of glycan holes promotes autologous NAb responses**

To test the impact of glycan holes on the induction of autologous NAbs, rabbits were immunized with the AMC011 Δ130Δ289 and AMC016 Δ130Δ289 trimers, as well as their parental counterparts. In the same study, a group of rabbits received the B41 trimer; data from this group, but not the other four, have been described previously (19). To allow comparability, sera from the B41 group were re analyzed in the same assays as for the AMC011 and AMC016 groups. Sera from week 22, two weeks after the third immunization, were assessed for autologous neutralization against the sequence-matched virus (Fig. 5A and Supplemental file 1). Murine leukemia virus (MLV) served as a negative control. One serum sample in the AMC016 Δ130Δ289 group was excluded from analysis because it interfered with MLV infection (see figure legends and crossed values in Supplemental file 1). Note that the GLA-LSQ adjuvant used in this study is now known to support SOSIP trimer immunogenicity inefficiently, which accounts for lower autologous NAb titers against B41 and AMC011 than we reported previously (2, 3, 19).

The parental AMC011 and AMC016 SOSIP trimers induced NAbs against the autologous viruses weakly and inconsistently; the median $ID_{50}$ values of 20 were not greater than the assay sensitivity limit (Fig. 5B; for individual values see Supplemental file 1). The glycan mutant trimers induced higher autologous titer (median $ID_{50}$ of 93 and 69 for AMC011 Δ130Δ289 and AMC016 Δ130Δ289, respectively; p=0.0079 for comparison of AMC011

SOSIP *versus* AMC011 Δ130Δ289 SOSIP; not significant for AMC016 SOSIP *versus* AMC016 Δ130Δ289 SOSIP).

The autologous NAb titers for the AMC011 and AMC016 parental trimer groups (median $ID_{50}$ of <20 for both groups) were also significantly lower than for the B41 trimer group (median $ID_{50}$ of 63 for B41 immunized animals; p=0.0476 *versus* either AMC011 or AMC016 parental trimers). The B41 autologous NAb titers were, however, similar to those induced by the AMC011 Δ130Δ289 and AMC016 Δ130Δ289 trimers (Fig. 5B). The NAbs induced by the AMC011 Δ130Δ289 and AMC016 Δ130Δ289 trimers did not neutralize the parental AMC011 and AMC016 viruses, implying that they were indeed targeting the glycan holes (median $ID_{50}$ of 20 and 26, respectively; see Supplemental file 1).

The analyses were then extended to include the AMC011 and AMC016 Δ289 virus variants. For each genotype, the median $ID_{50}$ value was defined as 100% for the Δ130Δ289 virus. Compared with this benchmark, the titers against the Δ289 virus were 66% and 70% for AMC011 Δ130Δ289 and AMC016 Δ130Δ289 immunized animals, respectively (analysis based on Fig. 5C). Thus, the data imply that the N289 glycan hole plays a major role in the induction of autologous NAbs.

In a further analysis, we found that sera from the AMC016 Δ130Δ289 trimer-immunized rabbits cross-neutralized the AMC011 Δ289 and Δ130Δ289 virus variants (median $ID_{50}$ values of 66 and 113, respectively; Fig. 5D and Supplemental file 1). But the AMC011 Δ130Δ289- and B41-trimer sera did not, however, cross-neutralize the AMC016 glycan-deleted virus variants (the median $ID_{50}$ values of 20 in all cases were not greater than the assay detection limit). The AMC011 and AMC016 Δ130Δ289 immunization sera also did not neutralize the B41 virus (median $ID_{50}$ values of 20). Thus, the induction of cross-reactive NAb responses, even against very similar glycan holes, remains challenging.

**Diverse SOSIP trimers induce different levels of autologous neutralization**

Based on the findings outlined above, we hypothesized that the number of missing PNGS influences the ability of trimers to induce autologous NAbs against glycan holes. To test this hypothesis, we analyzed a large panel of sera from rabbits immunized with one of 11 SOSIP trimers derived from different subtypes, with varying numbers of missing conserved PNGS (0 to 4) (Supplemental file 2). Specifically, we assessed the ability of the various trimers, formulated in ISCOMATRIX adjuvant, to induce autologous NAbs.

The trimer and virus genotypes were as follows (see Supplemental file 2 for details): BG505 (subtype A); AMC008, AMC009, AMC011, AMC016, AMC018, B41, TRJO

(subtype B); ZM197M, DU422, CZA97.012 (subtype C). The AMC011, AMC016, AMC011 Δ130Δ289, AMC016 Δ130Δ289 and B41 trimer immunogenicity data that are described in Fig. 5 were not included in this analysis as the adjuvant was different. Instead, published immunogenicity data of rabbits immunized with the AMC11 and B41 trimers in ISCOMATRIX adjuvant was included in the analysis presented in Fig. 5 and Fig. 8 (2, 3). Published data on autologous NAbs responses to the BG505, AMC008, AMC009 and ZM197M trimers were also used (2, 3, 27). The autologous NAb titers induced by the AMC016 and AMC018 trimers, with ISCOMATRIX adjuvant, have not been reported elsewhere.

The cryoEM structures of the AMC016 and AMC018 trimers were solved at 4.1 Å and 3.5 Å resolution, respectively, before they were used as immunogens (EMDB-24676 and PDB ID 7RSO for AMC016; EMDB-24675 and PDB ID 7RSN for AMC018). The structures of both trimers were solved when complexed with the CD4bs-directed bNAb PGV04 (PDB ID 6CRQ) (Fig. 6A, Fig. 6B, Fig.7 and Table 2) (28). Overlays of the structures of the AMC016 and AMC018 trimers with that of the BG505 SOSIP.664 trimer (PDB ID: 4ZMJ) showed that all three trimers are highly similar (Fig. 6C) (29). The C$\alpha$ root-mean-square deviation (RMSD) value, a quantitative measure for similarity between superimposed structures, was 1.1 Å for AMC016 *versus* BG505 in the gp120 subunit and 1.3 Å in the gp41 subunit, while the RMSD values for AMC018 *versus* BG505 were 1.0 Å, in gp120 and 1.5 Å in gp41.

The electron density for the AMC016 structure was sufficient to allow the building of 26 glycans out of 30 PNGS (Fig. 6D, glycans indicated in green), while we were able to build 16 glycans on the AMC018 structure out of 30 PNGS (Fig. 6D, glycans indicated in green). As the overall resolution increases, electron density corresponding to dynamic or flexible regions (e.g., uncoordinated N-linked glycans) becomes more diffuse, which prevents accurate model building of those regions. Thus, although the resolution of the AMC018 trimer structure was higher than that of the AMC016 trimer structure, the reduced electron density corresponding to PNGS in the AMC018 structure reduced the number of glycans that could be build.

The AMC016 and AMC18 viruses were categorized as tier 2 (Table 3). The corresponding AMC016 and AMC018 trimers were then tested as immunogens, as were the previously described DU422, CZA97.012 and TRJO trimers (see Material and Methods and Supplemental file 2) (18, 30, 31). In both studies, rabbits (n=5) were immunized at week 0, 4 and 20, with ISCOMATRIX used as the adjuvant. The median autologous NAb $ID_{50}$ values

measured at week-22 were 30, 39, 42, 401 and 719 for AMC016, AMC018, DU422, CZA97.012 and TRJO respectively (Fig. 8A, red squares and Supplemental file 2). The previously reported median $ID_{50}$ values for AMC009, AMC011, ZM197M, AMC008, B41 and BG505 are 20, 33, 67, 240, 1048, and 4561, respectively (Fig. 8A, grey spheres and Supplemental file 2) (2, 3, 27).

Autologous NAb titers could be influenced by various factors. Holes in the glycan shield, created by the absence of conserved PNGS, have been shown to promote autologous NAb induction (17, 26). We found a positive correlation between the number of missing PNGS and the median autologous NAb titers (Spearman r=0.6913; 95% CI=[0.1361-0.9160]; p=0.022). When inspecting the data, however, we noted substantial differences in the autologous NAb responses of trimers that each had the same number of missing PNGS (e.g., TRJO *versus* AMC009) (see Fig. 8A).

**The glycan hole area correlates with autologous neutralization**

The above analysis suggested that the number of missing PNGS affects autologous neutralization, but also that other factors may be relevant. The Los Alamos Glycan Shield Mapping tool (from here on abbreviated: Glycan Shield Mapping tool) allows for a more accurate prediction of the overall glycan hole area than just the number of missing PNGS (21). The tool takes the 3D structure of the Env trimer into account, as well as the shielding effect of neighboring glycans, assuming a radius of 10 Å for each glycan. Regions that are never shielded by glycans, such as the gp120-gp41 interface, the CD4 binding site and the fusion peptide, are excluded from the analysis. The focus is on conserved PNGS, which are present in >50% of HIV-1 group M viruses, and it is assumed that they are fully occupied.

We analyzed the above 11 SOSIP trimers using the Glycan Shield Mapping tool. The predicted glycan hole areas varied among the trimers (Fig. 8B and Supplemental file 2). The areas were relatively small (<200 $Å^2$) for AMC011, AMC009, DU422 and ZM197M (33, 170, 156, 156 $Å^2$); intermediate (<200-1000 $Å^2$) for AMC016, TRJO and AMC018 (218, 286, 803 $Å^2$); and large (>1000 $Å^2$) for AMC008, B41, CZA97.012 and BG505 (1120, 1641, 1671, 2401 $Å^2$). We found a positive correlation between the glycan hole area and the median autologous NAb titers (Spearman r=0.7062; 95% CI= [0.1645-0.9206]; p=0.019).

The tool also allows us to assess the individual surface area that is exposed by the absence of a conserved PNGS. The differences between the contributions to the overall glycan hole area made by N130 and N289 were analyzed, based on trimers that miss the two PNGS either naturally or by design. The absence of the N130 PNGS from DU422,

CZA97.012, AMC011 Δ130Δ289, AMC016 Δ130Δ289 and BG505 trimers did not generate a glycan hole, but created a very small hole on DU422 and B41 trimers (24.8 $Å^2$ for both) (Fig. 9, light grey). In contrast, the absence of N289 PNGS created a large glycan hole (1461 $Å^2$ for B41, AMC011 Δ130Δ289 and BG505; and 1211 $Å^2$ for AMC016 Δ130Δ289) (Fig. 9, dark grey). The above estimations are consistent with our finding that the hole created at N289 strongly influenced how autologous NAbs were induced by the AMC011 Δ130Δ289 and AMC016 Δ130Δ289 trimers (see Fig. 5C). They are also consistent with observations that the N130 site and the nearby region are not immunogenic on B41 and BG505 trimers (17, 18, 26, 32). However, as the autologous NAb titers were only analyzed in detail for the B41 and BG505 trimers, it is possible that the N130 glycan hole may be immunogenic on other trimers.

**The glycan hole area is a predictor for the induction of autologous neutralization**

Factors other than the number of missing PNGS and glycan hole area that might affect the induction of autologous NAbs, are best studied in combination, to supplement the simple correlation analyses described above. These possibly contributory factors include the neutralization tier categorization and genetic subtype of the trimer immunogen and the corresponding test virus (see Supplemental file 2). Trimer stability, for which $T_m$ values are a surrogate, may also be relevant, as immunogenic, non-neutralization epitopes become accessible if trimers dissociate into dimers and monomers.

We performed a linear regression analysis to study the above factors (Fig. 10A). The analysis was based on the median $ID_{50}$ values for the 11 SOSIP trimers shown in Fig. 8 (for individual values see Supplemental file 2). The log values of the autologous neutralization data were fitted to a generalized linear model that included the following predictor variables: neutralization tier categorization, genetic subtype, $T_m$, number of missing PNGS and log glycan hole area. The estimated 95% confidence intervals of the regression coefficients for tier, subtype, $T_m$ and the number of missing PNGS included zero (Fig. 10B). Hence, these four predictors are unlikely to influence autologous neutralization. In contrast, the mean regression coefficient of the glycan hole area was 0.67, suggesting a positive correlation. Although the estimated 95% confidence interval for glycan hole area is above zero, the interval is relatively wide, with a lower bound near zero (95% CI = [0.016, 1.322]). Hence, there is a degree of uncertainty about the influence of glycan hole area on autologous neutralization.

## Discussion

We establish here that the area of glycan holes, created when conserved PNGS are missing, influences the induction of autologous NAbs by native-like HIV-1 SOSIP trimers. We also describe here a new SOSIP trimer, AMC016 SOSIP.v4.2, as well as high-resolution cryoEM structures for the AMC16 and AMC018 trimers, adding to the repertoire of stable and native-like Env subtype B trimers.

The engineered knock-out of the PNGS at N130 and N289 had subtle impacts on glycan composition and occupancy. The changes were mostly localized on the trimer apex, near N130, and in the oligomannose patch, near N289. The reduction in $Man_9$ content of surrounding glycans suggests that the accessibility of ER α-mannosidase is increased when a PNGS is removed (16). Greater access to oligosaccharyltransferase (OST) might account for the increased occupancy of the N141 site at the trimer apex. The slightly reduced occupancy of N136 for AMC011 Δ130Δ289 is harder to explain, although it is known that OST can sometimes skip over one or more PNGS when several of them are located close together in the primary sequence (23). Our data show how the same glycan deletion on SOSIP trimers with similar characteristics can have a similar effect on the overall glycan shield, but different effects at the site-specific level. The individual *env* sequence as well as how the trimer folds (i.e., its structure and conformation) all seem to play a role.

The engineered or natural absence of a conserved PNGS creates glycan holes of different sizes on different SOSIP trimers. Deleting N130 does not create a measurable glycan hole or only yields a very small one, as was reported previously for the BG505 SOSIP trimer (21). The structure and dense local glycosylation of the V1 loop and the occupancy and composition of the neighboring glycans probably work together to create redundancy in that region of the glycan shield. Conversely, the absence of the N289 PNGS created a large glycan hole on all the SOSIP trimers we studied. That observation is consistent with how the autologous NAb response in animals immunized with B41 and BG505 SOSIP trimers is dominated by antibodies against the N289 glycan hole, and not its N130 counterpart (18). Where a missing PNGS is located within the overall glycan network matters from the perspective of inducing autologous NAbs.

We found that glycan hole area is positively correlated with autologous neutralization titer. Furthermore, the glycan hole area is a better predictor for NAb induction than the number of missing PNGS, although the two factors are clearly related. This relationship highlights the importance of missing PNGS at sites that are not conserved, as the resulting glycan holes can create immunodominant epitopes for narrow specificity NAbs. However, our

analyses were unable to explain all the variation in the Nab response. An explanation might be the variation in how autologous NAbs are induced. The inherent immunogenicity of the lining and base of a glycan hole and how accessible it is, the extent to which the compactness of a trimer affects epitope access more generally, the incomplete occupancy of various PNGS, and other factors are probably also relevant to various and not readily quantifiable extents.

Our analysis has limitations. First, the Glycan Shield Mapping tool assumes full occupancy, which is not the case for every PNGS on every trimer (33). A NxS motif is less likely to be glycosylated than NxT, and PNGS near the trimer base are generally relatively under-occupied (3, 23). Second, PNGS underoccupancy is more pronounced on soluble, recombinant trimers than on virus-associated Env (34, 35). Hence, antibodies induced by under-occupied PNGS are not detected in neutralization assays, except when tested against a mutant virus from which the PNGS is knocked out (23, 34). An example is the N611-directed antibodies induced by BG505 SOSIP trimers on which N611 is underoccupied (23, 36). Third, antibodies elicited by knocking-out conserved glycans were assumed to be able to cross-neutralize viruses that miss the same glycans. However, our neutralization data with B41 indicates, that this is not always the case. This is in line with the finding that SOSIP trimers, sharing the same glycan holes, can induce distinct autologous NAbs (26).

Nevertheless, the data presented here can guide the identification and assessment of potential new native-like trimer vaccine candidates and facilitate the selection of *env* sequences with certain qualities, such as a complete glycan shield or the presence of specific glycan holes. Our findings highlight the possibility to modify trimers by creating glycan holes and focus the immune response on desired epitopes. This can be used in prime-boost strategies, for example as components of germline-targeting approaches (37–39). For example, precursor VRC01 B cells can be activated using germline-targeting immunogens that lack glycans around the CD4bs (39), while it can be envisaged that subsequent ‘shaping’ and ‘polishing’ immunogen have gradually more complete glycan shields to mature responses to recognize the epitopes in the context of glycans.

## Materials and Methods

### Design and expression of Env SOSIP trimers

The parental SOSIP trimers, AMC011 SOSIP.v5.2 and AMC016 SOSIP.v4.2 were derived from subtype B virus-infected participants of the ACS on HIV/AIDS, who enrolled in the men having sex with men (MSM) cohort (40). The design and characterization of AMC011 SOSIP.v5.2 have been described elsewhere, while the AMC016 SOSIP.v4.2 trimer is described below (3). N130 and N289 were knocked out from both SOSIP trimers by site-directed mutagenesis (QuikChange II kit, Agilent Technologies) as described (5, 41). The mutated amino acids are indicated in Fig. 2A. Both trimers were expressed by transient transfection in HEK-293F cells and purified by PGT145 affinity chromatography (2, 5). The design and characteristics of the SOSIP trimers used in Fig. 8 were published: AMC009 SOSIP.v5.2 (3), AMC008 SOSIP.v4.2 (2), B41 SOSIP.v4.1 (25), BG505 SOSIP.v4.2 and v5.2 (2, 42), CZA97.012 SOSIP.664 (31), DU422 SOSIP.664 (30) and ZM197M SOSIP.v4.2 and v5.2 (42). TRJO SOSIP.v5.2 will be described in Cottrell et al. (manuscript in preparation). The AMC016 SOSIP.v4.2 trimer was based on an *env* sequence that was isolated at month 9 post-seroconversion from individual H19974, who did not develop bNAbs. The *env* sequence used to generate the AMC018 SOSIP.v4.2 trimer was isolated at month 3 post-seroconversion from individual H19961, who also did not develop bNAbs. The genes encoding the AMC016 and AMC018 SOSIP.v4.2 constructs were designed as described previously (2, 5). The codon-optimized env genes were obtained from GenScript (Piscataway, NJ), cloned into the pPPI4 expression vector, expressed in HEK-293F cells and affinity-purified with the bNAb PGT145 (2, 5). A D7324 epitope-tag sequence (GSAPTKAKRRVVQREKR) was introduced to the AMC016 SOSIP.v4.2 sequence, C-terminally of residue 664 in $gp41_{ECTO}$, to allow analysis in a D7324-mAb-capture ELISA and DSC.

### Blue Native-PAGE and SDS PAGE

SOSIP trimers were analyzed on blue native-PAGE and SDS-PAGE gels to check trimerization and cleavage by furin (5).

### D7324-capture ELISA

This ELISA for characterizing PGT145-purified SOSIP trimer was performed as described previously (5). Briefly, Microlon 96-wells plates (Greiner Bio-One, Alphen aan den Rijn, The

Netherlands) were coated overnight with sheep polyclonal antibody D7324 (Aalto Bioreagents, Dublin, Ireland) at 10 µg/ml. Purified D7324-tagged SOSIP trimers (2.75 µg/ml) were captured on the plate and the binding of a panel of bNAbs and non-neutralizing antibody 17b tested. Goat-anti-human HRP-labeled IgG was used as a secondary antibody.

**Differential scanning calorimetry**

Thermal denaturation was probed with a nano-DSC calorimeter (TA Instruments, Etten-Leur, The Netherlands) and a two-state scaled model applied to determine the thermal denaturation (2). DSC experiments where performed with the D7324-tagged SOSIP protein; the presence of the D7324-tag does not influence $T_m$ values (2).

**Negative-stain electron microscopy and image processing**

The imaging and processing of the SOSIP trimers were described previously (2).

**N-glycan profiling using HILIC-UPLC**

N-linked glycan profiling using HILIC-UPLC was described in detail previously (13, 23). N-linked glycans were released from trimers in-gel by digestion with PNGase F (New England Biolabs). The released glycans were fluorescently labeled with procainamide and analyzed with a Glycan BEH Amide column (2.1 mm x 100 mm, 1.7 mM, Waters) in a Waters Acquity H-Class UPLC instrument, and the fluorescence measured. To determine the relative abundance of oligomannose-type glycans, labeled glycans were digested for 16 h at 37°C with Endoglycosidase H (Endo H; New England Biolabs). The digested glycans were purified on a PVDF protein-binding membrane plate (Millipore) and then analyzed.

**Site-specific glycan analysis using mass spectrometry**

N-linked glycan composition and occupancy at every present PNGS was analyzed with mass spectrometry, as previously described (23). Some of the PNGS frequently present low intensity glycoproteins. In order to still obtain information on these sites, the glycans that are present on the glycopeptides were homogenized to boost the intensity of these peptides (23). In this way, the ratios of oligomannose glycans / complex glycans / unoccupied PNGS can be determined, but fine processing information is lost.

**Single particle cryo-electron microscopy**

The AMC016 SOSIP.v4.2 and AMC018 SOSIP.v4.2 trimers were incubated with the PGV04 Fab at a 2-fold molar excess of Fab/protomer, overnight at room temperature. The complexes were purified using a Superose 6 10/300 column (GE healthcare) in TBS to remove unbound Fab. The purified complexes were mixed with n-dodecyl-D-maltoside to a final concentration of 675 μM and applied to C-Flat grids (CF-2/2-4C, Electron Microscopy Sciences, Protochips, Inc.). The grid had been plasma cleaned for 5 s using a mixture of Ar/O2 (Gatan Solarus 950 Plasma system). Samples were manually blotted using filter paper and then immediately plunged into liquid ethane using a manual freeze plunger. Data were collected via the Leginon interface on a FEI Titan Krios operating at 300 keV mounted with a Gatan K2 direct electron detector in counting mode at 22,500 × nominal magnification resulting in a calibrated pixel size of 1.31 Å/pix at the objective level (43). Dose rate and additional data collection parameters are reported in S1 Table. Movies were imported into cryoSPARC v2 and frames were aligned using full-frame motion correction (44). The contrast transfer function (CTF) for each aligned micrograph was estimated using Gctf (45). The HIV Env portion of the BG505 SOSIP.664 trimer (PDB ID: 5ACO) was converted to an EM density and low pass filtered to 40 Å using pdb2mrc and subsequently used as a template for particle picking within cryoSPARC v2 (44, 46, 47). 2D classification, Ab-initio 3D reconstruction, homogenous 3D refinement, and local motion correction were conducted with cryoSPARC v2 (44). Per-particle CTF estimation was conducted using Gctf (45). Local resolution maps were generated using cryoSPARC v2 (44). Initial molecular models for the AMC016 SOSIP.v4.2 and AMC018 SOSIP.v4.2 trimer were generated using the Modeller homology modeling plug-in UCSF Chimera (48, 49). The templates for AMC016 SOSIP.v4.2 were the JR-FL Env structures (PDB ID: 5FYK (gp120) and PDB ID: 5FUU (gp41)) (9, 50). The template for AMC018 SOSIP.v4.2 was the AMC009 SOSIP.v4.2 Env structure (PDB ID: 6VO3) (3). Models were docked into corresponding EM density map along with the PGV04 Fv (PDB ID: 6CRQ) using UCSF Chimera (49). Regions not supported by density were removed and N-linked glycans were added using Coot (51). The models were iteratively refined into the EM density maps using RosettaRelax and Coot (52, 53). Glycan structures were validated using Privateer and the overall structures were evaluated using EMRinger and MolProbity (54–56).

**Rabbit immunizations**

Rabbit immunizations with AMC016 SOSIP.v4.2, AMC016 SOSIP.v4.2 Δ130Δ289, AMC011 SOSIP.v5.2, AMC011 SOSIP.v5.2 Δ130Δ289 and B41 SOSIP.v4.1 trimers were carried out under approval number C0026-17, under subcontract at Covance (Denver, PA,

USA). Female New Zealand White rabbits (5 per group) were immunized intramuscularly with 30 µg of SOSIP trimer at week 0, 4 and 20, with GLA-LSQ adjuvant (IDRI, Seattle, WA, obtained via the BMGF's collaborative network). The B41 trimer experiment has been published, but the sera were re-analyzed alongside other sera from same study to generate comparable data (see Fig 3) (19). We learned post hoc that GLA-LSQ is an inefficient adjuvant, such that NAb titers are lower in this experiment than in previously published experiments were a different adjuvant was used (2, 3). Sera from week 22 in the present (GLA-LSQ) experiment were used to derive the autologous NAb responses as plotted in Fig. 5, but they were excluded from the analysis in Fig. 8 and Fig. 10 for non-comparability reason. All the week 22 NAb titer data shown in Fig. 8 and Fig. 10 were derived from experiments in which the adjuvant was ISCOMATRIX. NAb responses to the AMC009, AMC011, ZM197M, AMC008, B41 and BG505 trimers (indicated in grey spheres in Fig. 8) were previously published (2, 3, 27).

The immunogenicity of the AMC016 and AMC018 SOSIP.v4.2 trimers was assessed under approval number C0048-15 at Covance. The data are presented in Fig. 8, indicated in dark red squares, and Fig. 10. The protocol was identical to that described above, except that 22 µg of trimer was used with ISCOMATRIX adjuvant (CSL Ltd., Parkville, VIC, Australia). In Covance study PA0064-16, the TRJO SOSIP.v5.2, DU422 SOSIP.664 and CZA97.012 SOSIP.664 trimers were used at 30 µg with ISCOMATRIX (data shown in dark red squares in Fig. 8 and Fig. 10). Sera samples of PA0064-16 were analyzed at DUMC, all other sere were analyzed at Amsterdam UMC. In both the C0048-15 and PA0064-16 studies, the autologous NAb titers were determined using week 22 sera (for individual $ID_{50}$ values see Supplemental file 2).

**Neutralization assay and generation of infectious molecular clones**

A standard TZM-bl cell neutralization assay was used to measure the autologous NAb titers (2, 57–60). The AMC011 and AMC016 Δ289 and Δ130Δ289 viral variants were ordered as infectious molecular clones and virus infectivity quantified in a standard TZM-bl cell assay via titration. The deletion of the N130 and/or N289 glycans did not affect virus infectivity. The parental virus and the corresponding glycan variants neutralized VRC01 with a similar $IC_{50}$. These data are in line with previous findings that removal of most single PNGS, including the ones studies here, do not have a major impact on infectivity (61, 62). The other viruses (DU422, CZA97.012 and TRJO) used to analyze sera from the P0064-16 study have been described previously (18, 63). The AMC016 and AMC018 viruses were tested at DUMC

against serum pools and a panel of well-characterized antibodies, using a standard TZM-bl cell assay (63, 64).

**Statistical analyses**

NAb titers ($ID_{50}$) of groups in Fig. 5 were compared by the two-tailed Mann-Whitney *U* test. Spearman's rank correlation coefficients and p values (two-tailed) were calculated to determine the correlation between median autologous NAb titers and the number of missing PNGS or the glycan hole area. Both tests were performed in GraphPad Prism 8. To analyze the data in Fig. 10 we performed a log transform of the median autologous neutralization value of each trimer to reduce the right skewness of the data. The $T_m$ values of the ZM197M and BG505 SOSIP.v4.2 and v.5.2 variants were averaged ($T_m$ of 62.6°C *versus* 69.2°C for ZM197M variants and 69.3°C *versus* 75.0°C for BG505 variants, respectively). We then fitted the neutralization values (median $ID_{50}$) ($Y_{neut}$) to a generalized linear model that included predictor variables such as tier categorization ($X_{tier}$), subtype ($X_{subtype}$), midpoint of thermal denaturation ($X_{T_m}$), number of missing PNGs ($X_{PNGS}$) and log glycan hole area ($X_{glycan}$):

$$Y_{neut} = \sum_i \beta_i X_i + c$$

where $i = \{\text{tier, subtype, } T_m\text{, PNGS, glycan}\}$. We encoded the categorical predictors $X_{subtype}$ as subtype A = 0, subtype B = 1 and subtype C = 2; $X_{tier}$ as 0 when tier = 2 and 1 when tier = 1B. Computing eigenvalues on the covariance matrix between all predictor variables, we assessed that there is no multicollinearity between them. The model was fitted using the statsmodels package in Python (60).

**Data availability**

The cryo-EM reconstruction and the molecular model described here have been deposited in the Electron Microscopy Data Bank and Protein Data Bank, under the following accession codes: AMC016 SOSIP.v4.2 (EMDB-24676; PDB ID 7RSO) and AMC018 SOSIP.v4.2 (EMDB-24675; PDB ID 7RSN).

## Acknowledgements

We thank Cheng Cheng of the NIAID Vaccine Research Center for the gift of the Adjuplex-based adjuvant. We thank Ronald Derking and Kwinten Sliepen for support and helpful discussions and the participants of Amsterdam Cohort Studies on HIV and AIDS for providing their samples.

## References


1. Haynes BF, Burton DR. 2017. Developing an HIV vaccine. Science (80- ) 355:1129–1130.
2. de Taeye SW, Ozorowski G, Torrents de la Peña A, Guttman M, Julien JP, van den Kerkhof TLGM, Burger JA, Pritchard LK, Pugach P, Yasmeen A, Crampton J, Hu J, Bontjer I, Torres JL, Arendt H, Destefano J, Koff WC, Schuitemaker H, Eggink D, Berkhout B, Dean H, Labranche C, Crotty S, Crispin M, Montefiori DC, Klasse PJ, Lee KK, Moore JP, Wilson IA, Ward AB, Sanders RW. 2015. Immunogenicity of Stabilized HIV-1 Envelope Trimers with Reduced Exposure of Non-neutralizing Epitopes. Cell 163:1702–1715.
3. Schorcht A, van den Kerkhof TLGM, Cottrell CA, Allen JD, Torres JL, Behrens A-J, Schermer EE, Burger JA, de Taeye SW, Torrents de la Peña A, Bontjer I, Gumbs S, Ozorowski G, LaBranche CC, de Val N, Yasmeen A, Klasse PJ, Montefiori DC, Moore JP, Schuitemaker H, Crispin M, van Gils MJ, Ward AB, Sanders RW. 2020. Neutralizing Antibody Responses Induced by HIV-1 Envelope Glycoprotein SOSIP Trimers Derived from Elite Neutralizers. J Virol 94:e01214-20.
4. Klasse PJ, Ketas TJ, Cottrell CA, Ozorowski G, Debnath G, Camara D, Francomano E, Pugach P, Ringe RP, LaBranche CC, van Gils MJ, Bricault CA, Barouch DH, Crotty S, Silvestri G, Kasturi S, Pulendran B, Wilson IA, Montefiori DC, Sanders RW, Ward AB, Moore JP. 2018. Epitopes for neutralizing antibodies induced by HIV-1 envelope glycoprotein BG505 SOSIP trimers in rabbits and macaques. PLoS Pathog 14:1–20.
5. Sanders RW, Derking R, Cupo A, Julien JP, Yasmeen A, de Val N, Kim HJ, Blattner C, de la Peña AT, Korzun J, Golabek M, de los Reyes K, Ketas TJ, van Gils MJ, King CR, Wilson IA, Ward AB, Klasse PJ, Moore JP. 2013. A Next-Generation Cleaved, Soluble HIV-1 Env Trimer, BG505 SOSIP.664 gp140, Expresses Multiple Epitopes for Broadly Neutralizing but Not Non-Neutralizing Antibodies. PLoS Pathog 9:e1003618.
6. Ward AB, Wilson IA. 2017. The HIV-1 envelope glycoprotein structure: nailing down a moving target. Immunol Rev 275:21–32.
7. Crispin M, Ward AB, Wilson IA. 2018. Structure and Immune Recognition of the HIV Glycan Shield. Annu Rev Biophys 47:499–523.
8. Klasse PJ, Ozorowski G, Sanders RW, Moore JP. 2020. Env Exceptionalism: Why Are HIV-1 Env Glycoproteins Atypical Immunogens? Cell Host Microbe 27:507–518.
9. Stewart-Jones GBE, Soto C, Lemmin T, Chuang G-Y, Druz A, Kong R, Thomas P V, Wagh K, Zhou T, Behrens A-J, Bylund T, Choi CW, Davison JR, Georgiev IS, Joyce

MG, Kwon Y Do, Pancera M, Taft J, Yang Y, Zhang B, Shivatare SS, Shivatare VS, Lee C-CD, Wu C-Y, Bewley CA, Burton DR, Koff WC, Connors M, Crispin M, Baxa U, Korber BT, Wong C-H, Mascola JR, Kwong PD. 2016. Trimeric HIV-1-Env Structures Define Glycan Shields from Clades A, B, and G. Cell 165:813–26.

10. Mellquist JL, Kasturi L, Spitalnik SL, Shakin-Eshleman SH. 1998. The amino acid following an Asn-X-Ser/Thr sequon is an important determinant of N-linked core glycosylation efficiency. Biochemistry 37:6833–6837.

11. Kasturi L, Eshleman JR, Wunner WH, Shakin-Eshleman SH. 1995. The hydroxy amino acid in an Asn-X-Ser/Thr sequon can influence N-linked core glycosylation efficiency and the level of expression of a cell surface glycoprotein. J Biol Chem 270:14756–14761.

12. Behrens A-J, Vasiljevic S, Pritchard LK, Harvey DJ, Andev RS, Krumm SA, Struwe WB, Cupo A, Kumar A, Zitzmann N, Seabright GE, Kramer HB, Spencer DIR, Royle L, Lee JH, Klasse PJ, Burton DR, Wilson IA, Ward AB, Sanders RW, Moore JP, Doores KJ, Crispin M. 2016. Composition and Antigenic Effects of Individual Glycan Sites of a Trimeric HIV-1 Envelope Glycoprotein. Cell Rep 14:2695–2706.

13. Pritchard LK, Spencer DIR, Royle L, Bonomelli C, Seabright GE, Behrens AJ, Kulp DW, Menis S, Krumm SA, Dunlop DC, Crispin DJ, Bowden TA, Scanlan CN, Ward AB, Schief WR, Doores KJ, Crispin M. 2015. Glycan clustering stabilizes the mannose patch of HIV-1 and preserves vulnerability to broadly neutralizing antibodies. Nat Commun 6:7479.

14. Doores KJ, Bonomelli C, Harvey DJ, Vasiljevic S, Dwek RA, Burton DR, Crispin M, Scanlan CN. 2010. Envelope glycans of immunodeficiency virions are almost entirely oligomannose antigens. Proc Natl Acad Sci U S A 107:13800–13805.

15. Bonomelli C, Doores KJ, Dunlop DC, Thaney V, Dwek RA, Burton DR, Crispin M, Scanlan CN. 2011. The glycan shield of HIV is predominantly oligomannose independently of production system or viral clade. PLoS One 6:e23521.

16. Seabright GE, Cottrell CA, van Gils MJ, D'addabbo A, Harvey DJ, Behrens AJ, Allen JD, Watanabe Y, Scaringi N, Polveroni TM, Maker A, Vasiljevic S, de Val N, Sanders RW, Ward AB, Crispin M. 2020. Networks of HIV-1 Envelope Glycans Maintain Antibody Epitopes in the Face of Glycan Additions and Deletions. Structure 28:897-909.e6.

17. McCoy LE, van Gils MJ, Ozorowski G, Messmer T, Briney B, Voss JE, Kulp DW, Macauley MS, Sok D, Pauthner M, Menis S, Cottrell CA, Torres JL, Hsueh J, Schief

WR, Wilson IA, Ward AB, Sanders RW, Burton DR. 2016. Holes in the Glycan Shield of the Native HIV Envelope Are a Target of Trimer-Elicited Neutralizing Antibodies. Cell Rep 16:2327–2338.

18. Klasse PJ, LaBranche CC, Ketas TJ, Ozorowski G, Cupo A, Pugach P, Ringe RP, Golabek M, van Gils MJ, Guttman M, Lee KK, Wilson IA, Butera ST, Ward AB, Montefiori DC, Sanders RW, Moore JP. 2016. Sequential and Simultaneous Immunization of Rabbits with HIV-1 Envelope Glycoprotein SOSIP.664 Trimers from Clades A, B and C. PLoS Pathog 12:1–31.

19. Ringe RP, Pugach P, Cottrell CA, LaBranche CC, Seabright GE, Ketas TJ, Ozorowski G, Kumar S, Schorcht A, van Gils MJ, Crispin M, Montefiori DC, Wilson IA, Ward AB, Sanders RW, Klasse PJ, Moore JP. 2019. Closing and Opening Holes in the Glycan Shield of HIV-1 Envelope Glycoprotein SOSIP Trimers Can Redirect the Neutralizing Antibody Response to the Newly Unmasked Epitopes. J Virol 93:1–26.

20. Zhou T, Doria-Rose NA, Cheng C, Stewart-Jones GBE, Chuang GY, Chambers M, Druz A, Geng H, McKee K, Kwon Y Do, O'Dell S, Sastry M, Schmidt SD, Xu K, Chen L, Chen RE, Louder MK, Pancera M, Wanninger TG, Zhang B, Zheng A, Farney SK, Foulds KE, Georgiev IS, Joyce MG, Lemmin T, Narpala S, Rawi R, Soto C, Todd JP, Shen CH, Tsybovsky Y, Yang Y, Zhao P, Haynes BF, Stamatatos L, Tiemeyer M, Wells L, Scorpio DG, Shapiro L, McDermott AB, Mascola JR, Kwong PD. 2017. Quantification of the Impact of the HIV-1-Glycan Shield on Antibody Elicitation. Cell Rep 19:719–732.

21. Wagh K, Kreider EF, Li Y, Barbian HJ, Learn GH, Giorgi E, Hraber PT, Decker TG, Smith AG, Gondim M V, Gillis L, Wandzilak J, Chuang GY, Rawi R, Cai F, Pellegrino P, Williams I, Overbaugh J, Gao F, Kwong PD, Haynes BF, Shaw GM, Borrow P, Seaman MS, Hahn BH, Korber B. 2018. Completeness of HIV-1 Envelope Glycan Shield at Transmission Determines Neutralization Breadth. Cell Rep 25:893-908.e7.

22. Wagh K, Hahn BH, Korber B. 2020. Hitting the sweet spot: Exploiting HIV-1 glycan shield for induction of broadly neutralizing antibodies. Curr Opin HIV AIDS 15:267–274.

23. Derking R, Allen JD, Cottrell CA, Sliepen K, Seabright GE, Lee WH, Aldon Y, Rantalainen K, Antanasijevic A, Copps J, Yasmeen A, Cupo A, Cruz Portillo VM, Poniman M, Bol N, van der Woude P, de Taeye SW, van den Kerkhof TLGM, Klasse PJ, Ozorowski G, van Gils MJ, Moore JP, Ward AB, Crispin M, Sanders RW. 2021.

Enhancing glycan occupancy of soluble HIV-1 envelope trimers to mimic the native viral spike. Cell Rep 35:108933.

24. Sanders RW, Moore JP. 2021. Virus vaccines: proteins prefer prolines. Cell Host Microbe 29:327–333.

25. Pugach P, Ozorowski G, Cupo A, Ringe R, Yasmeen A, de Val N, Derking R, Kim HJ, Korzun J, Golabek M, de los Reyes K, Ketas TJ, Julien J-P, Burton DR, Wilson IA, Sanders RW, Klasse PJ, Ward AB, Moore JP. 2015. A Native-Like SOSIP.664 Trimer Based on an HIV-1 Subtype B env Gene . J Virol 89:3380–3395.

26. Yang YR, McCoy LE, van Gils MJ, Andrabi R, Turner HL, Yuan M, Cottrell CA, Ozorowski G, Voss J, Pauthner M, Polveroni TM, Messmer T, Wilson IA, Sanders RW, Burton DR, Ward AB. 2020. Autologous Antibody Responses to an HIV Envelope Glycan Hole Are Not Easily Broadened in Rabbits. J Virol 94:e01861-19.

27. Torrents de la Peña A, de Taeye SW, Sliepen K, LaBranche CC, Burger JA, Schermer EE, Montefiori DC, Moore JP, Klasse PJ, Sanders RW. 2018. Immunogenicity in Rabbits of HIV-1 SOSIP Trimers from Clades A, B, and C, Given Individually, Sequentially, or in Combination. J Virol 92:e01957-17.

28. Schiffner T, Pallesen J, Russell RA, Dodd J, de Val N, LaBranche CC, Montefiori D, Tomaras GD, Shen X, Harris SL, Moghaddam AE, Kalyuzhniy O, Sanders RW, McCoy LE, Moore JP, Ward AB, Sattentau QJ. 2018. Structural and immunologic correlates of chemically stabilized HIV-1 envelope glycoproteins. PLoS Pathog 14:1–30.

29. Do Kwon Y, Pancera M, Acharya P, Georgiev IS, Crooks ET, Gorman J, Joyce MG, Guttman M, Ma X, Narpala S, Soto C, Terry DS, Yang Y, Zhou T, Ahlsen G, Bailer RT, Chambers M, Chuang GY, Doria-Rose NA, Druz A, Hallen MA, Harned A, Kirys T, Louder MK, O'Dell S, Ofek G, Osawa K, Prabhakaran M, Sastry M, Stewart-Jones GBE, Stuckey J, Thomas P V., Tittley T, Williams C, Zhang B, Zhao H, Zhou Z, Donald BR, Lee LK, Zolla-Pazner S, Baxa U, Schön A, Freire E, Shapiro L, Lee KK, Arthos J, Munro JB, Blanchard SC, Mothes W, Binley JM, McDermott AB, Mascola JR, Kwong PD. 2015. Crystal structure, conformational fixation and entry-related interactions of mature ligand-free HIV-1 Env. Nat Struct Mol Biol 22:522–531.

30. Julien J-P, Lee JH, Ozorowski G, Hua Y, Torrents de la Peña A, de Taeye SW, Nieusma T, Cupo A, Yasmeen A, Golabek M, Pugach P, Klasse PJ, Moore JP, Sanders RW, Ward AB, Wilson IA. 2015. Design and structure of two HIV-1 clade C SOSIP.664 trimers that increase the arsenal of native-like Env immunogens. Proc Natl

Acad Sci 112:11947–11952.

31. Ringe RP, Yasmeen A, Ozorowski G, Go EP, Pritchard LK, Guttman M, Ketas TA, Cottrell CA, Wilson IA, Sanders RW, Cupo A, Crispin M, Lee KK, Desaire H, Ward AB, Klasse PJ, Moore JP. 2015. Influences on the Design and Purification of Soluble, Recombinant Native-Like HIV-1 Envelope Glycoprotein Trimers. J Virol 89:12189–12210.

32. Dingens AS, Pratap P, Malone K, Hilton SK, Ketas T, Cottrell CA, Overbaugh J, Moore JP, Klasse PJ, Ward AB, Bloom JD. 2021. High-resolution mapping of the neutralizing and binding specificities of polyclonal sera post hiv env trimer vaccination. Elife 10:1–32.

33. Wagh K, Bhattacharya T, Williamson C, Robles A, Bayne M, Garrity J, Rist M, Rademeyer C, Yoon H, Lapedes A, Gao H, Greene K, Louder MK, Kong R, Karim SA, Burton DR, Barouch DH, Nussenzweig MC, Mascola JR, Morris L, Montefiori DC, Korber B, Seaman MS. 2016. Optimal Combinations of Broadly Neutralizing Antibodies for Prevention and Treatment of HIV-1 Clade C Infection. PLoS Pathog 12:1–27.

34. Struwe WB, Chertova E, Allen JD, Seabright GE, Watanabe Y, Harvey DJ, Medina-Ramirez M, Roser JD, Smith R, Westcott D, Keele BF, Bess JW, Sanders RW, Lifson JD, Moore JP, Crispin M. 2018. Site-Specific Glycosylation of Virion-Derived HIV-1 Env Is Mimicked by a Soluble Trimeric Immunogen. Cell Rep 24:1958-1966.e5.

35. Cao L, Pauthner M, Andrabi R, Rantalainen K, Berndsen Z, Diedrich JK, Menis S, Sok D, Bastidas R, Park SKR, Delahunty CM, He L, Guenaga J, Wyatt RT, Schief WR, Ward AB, Yates JR, Burton DR, Paulson JC. 2018. Differential processing of HIV envelope glycans on the virus and soluble recombinant trimer. Nat Commun 9:3693.

36. Cottrell CA, van Schooten J, Bowman CA, Yuan M, Oyen D, Shin M, Morpurgo R, van der Woude P, van Breemen M, Torres JL, Patel R, Gross J, Sewall LM, Copps J, Ozorowski G, Nogal B, Sok D, Rakasz EG, Labranche C, Vigdorovich V, Christley S, Carnathan DG, Sather DN, Montefiori D, Silvestri G, Burton DR, Moore JP, Wilson IA, Sanders RW, Ward AB, van Gils MJ. 2020. Mapping the immunogenic landscape of near-native HIV-1 envelope trimers in non-human primates. PLoS Pathog 16:e1008753.

37. Steichen JM, Kulp DW, Tokatlian T, Escolano A, Dosenovic P, Stanfield RL, McCoy LE, Ozorowski G, Hu X, Kalyuzhniy O, Briney B, Schiffner T, Garces F, Freund NT, Gitlin AD, Menis S, Georgeson E, Kubitz M, Adachi Y, Jones M, Mutafyan AA, Yun

DS, Mayer CT, Ward AB, Burton DR, Wilson IA, Irvine DJ, Nussenzweig MC, Schief WR. 2016. HIV Vaccine Design to Target Germline Precursors of Glycan-Dependent Broadly Neutralizing Antibodies. Immunity 45:483–496.

38. Medina-Ramírez M, Garces F, Escolano A, Skog P, de Taeye SW, Del Moral-Sanchez I, McGuire AT, Yasmeen A, Behrens A-J, Ozorowski G, van den Kerkhof TLGM, Freund NT, Dosenovic P, Hua Y, Gitlin AD, Cupo A, van der Woude P, Golabek M, Sliepen K, Blane T, Kootstra N, van Breemen MJ, Pritchard LK, Stanfield RL, Crispin M, Ward AB, Stamatatos L, Klasse PJ, Moore JP, Nemazee D, Nussenzweig MC, Wilson IA, Sanders RW. 2017. Design and crystal structure of a native-like HIV-1 envelope trimer that engages multiple broadly neutralizing antibody precursors in vivo. J Exp Med 214:2573–2590.

39. Lin YR, Parks KR, Weidle C, Naidu AS, Khechaduri A, Riker AO, Takushi B, Chun JH, Borst AJ, Veesler D, Stuart A, Agrawal P, Gray M, Pancera M, Huang PS, Stamatatos L. 2020. HIV-1 VRC01 Germline-Targeting Immunogens Select Distinct Epitope-Specific B Cell Receptors. Immunity 53:840-851.e6.

40. Wolf F d., Lange JMA, Houweling JTM, Coutinbo RA, Scbellekens PT, Noordaa J v. d., Goudsmit J. 1988. Numbers of CD4+ Cells and the Levels of Core Antigens of and Antibodies to the Human Immunodeficiency Virus as Predictors of AIDS Among Seropositive Homosexual Men. J Infect Dis 158:615–622.

41. Ringe RP, Ozorowski G, Rantalainen K, Struwe WB, Matthews K, Torres JL, Yasmeen A, Cottrell CA, Ketas TJ, LaBranche CC, Montefiori DC, Cupo A, Crispin M, Wilson IA, Ward AB, Sanders RW, Klasse PJ, Moore JP. 2017. Reducing V3 Antigenicity and Immunogenicity on Soluble, Native-Like HIV-1 Env SOSIP Trimers. J Virol 91:e00677-17.

42. Torrents de la Peña A, Julien JP, de Taeye SW, Garces F, Guttman M, Ozorowski G, Pritchard LK, Behrens AJ, Go EP, Burger JA, Schermer EE, Sliepen K, Ketas TJ, Pugach P, Yasmeen A, Cottrell CA, Torres JL, Vavourakis CD, van Gils MJ, LaBranche C, Montefiori DC, Desaire H, Crispin M, Klasse PJ, Lee KK, Moore JP, Ward AB, Wilson IA, Sanders RW. 2017. Improving the Immunogenicity of Native-like HIV-1 Envelope Trimers by Hyperstabilization. Cell Rep 20:1805–1817.

43. Carragher B, Kisseberth N, Kriegman D, Milligan RA, Potter CS, Pulokas J, Reilein A. 2000. Leginon: An automated system for acquisition of images from vitreous ice specimens. J Struct Biol 132:33–45.

44. Punjani A, Rubinstein JL, Fleet DJ, Brubaker MA. 2017. CryoSPARC: Algorithms for

rapid unsupervised cryo-EM structure determination. Nat Methods 14:290–296.

45. Zhang K. 2016. Gctf: Real-time CTF determination and correction. J Struct Biol 193:1–12.

46. Ludtke SJ, Baldwin PR, Chiu W. 1999. EMAN: Semiautomated software for high-resolution single-particle reconstructions. J Struct Biol 128:82–97.

47. Lee JH, De Val N, Lyumkis D, Ward AB. 2015. Model building and refinement of a natively glycosylated HIV-1 Env protein by high-resolution cryoelectron microscopy. Structure 23:1943–1951.

48. Webb B, Sali A. 2016. Comparative protein structure modeling using MODELLER. Curr Protoc Protein Sci 2016:2.9.1-2.9.37.

49. Pettersen EF, Goddard TD, Huang CC, Couch GS, Greenblatt DM, Meng EC, Ferrin TE. 2004. UCSF Chimera - A visualization system for exploratory research and analysis. J Comput Chem 25:1605–1612.

50. Lee JH, Ozorowski G, Ward AB. 2016. Cryo-EM structure of a native, fully glycosylated, cleaved HIV-1 envelope trimer. Science (80- ) 351:1043–1048.

51. van Beusekom B, Wezel N, Hekkelman ML, Perrakis A, Emsley P, Joosten RP. 2019. Building and rebuilding N-glycans in protein structure models. Acta Crystallogr Sect D Struct Biol 75:416–425.

52. Emsley P, Lohkamp B, Scott WG, Cowtan K. 2010. Features and development of Coot. Acta Crystallogr Sect D Biol Crystallogr 66:486–501.

53. Dimaio F, Song Y, Li X, Brunner MJ, Xu C, Conticello V, Egelman E, Marlovits TC, Cheng Y, Baker D. 2015. Atomic-accuracy models from 4.5-Å cryo-electron microscopy data with density-guided iterative local refinement. Nat Methods 12:361–365.

54. Barad BA, Echols N, Wang RYR, Cheng Y, Dimaio F, Adams PD, Fraser JS. 2015. EMRinger: Side chain-directed model and map validation for 3D cryo-electron microscopy. Nat Methods 12:943–946.

55. Williams CJ, Headd JJ, Moriarty NW, Prisant MG, Videau LL, Deis LN, Verma V, Keedy DA, Hintze BJ, Chen VB, Jain S, Lewis SM, Arendall WB, Snoeyink J, Adams PD, Lovell SC, Richardson JS, Richardson DC. 2018. MolProbity: More and better reference data for improved all-atom structure validation. Protein Sci 27:293–315.

56. Agirre J, Iglesias-Fernández J, Rovira C, Davies GJ, Wilson KS, Cowtan KD. 2015. Privateer: Software for the conformational validation of carbohydrate structures. Nat Struct Mol Biol 22:833–834.

57. Li M, Gao F, Mascola JR, Stamatatos L, Polonis VR, Koutsoukos M, Voss G, Goepfert P, Gilbert P, Greene KM, Bilska M, Kothe DL, Salazar-Gonzalez JF, Wei X, Decker JM, Hahn BH, Montefiori DC. 2005. Human Immunodeficiency Virus Type 1 env Clones from Acute and Early Subtype B Infections for Standardized Assessments of Vaccine-Elicited Neutralizing Antibodies . J Virol 79:10108–10125.

58. Sarzotti-Kelsoe M, Bailer RT, Turk E, Lin C li, Bilska M, Greene KM, Gao H, Todd CA, Ozaki DA, Seaman MS, Mascola JR, Montefiori DC. 2014. Optimization and validation of the TZM-bl assay for standardized assessments of neutralizing antibodies against HIV-1. J Immunol Methods 409:131–146.

59. Montefiori DC. 2009. Measuring HIV neutralization in a luciferase reporter gene assay. Methods Mol Biol 485:395–405.

60. Mascola JR, D'Souza P, Gilbert P, Hahn BH, Haigwood NL, Morris L, Petropoulos CJ, Polonis VR, Sarzotti M, Montefiori DC. 2005. Recommendations for the Design and Use of Standard Virus Panels To Assess Neutralizing Antibody Responses Elicited by Candidate Human Immunodeficiency Virus Type 1 Vaccines. J Virol 79:10103–10107.

61. Wang W, Nie J, Prochnow C, Truong C, Jia Z, Wang S, Chen XS, Wang Y. 2013. A systematic study of the N-glycosylation sites of HIV-1 envelope protein on infectivity and antibody-mediated neutralization. Retrovirology 10:14.

62. Lavine CL, Lao S, Montefiori DC, Haynes BF, Sodroski JG, Yang X. 2012. High-Mannose Glycan-Dependent Epitopes Are Frequently Targeted in Broad Neutralizing Antibody Responses during Human Immunodeficiency Virus Type 1 Infection. J Virol 86:2153–2164.

63. Seaman MS, Janes H, Hawkins N, Grandpre LE, Devoy C, Giri A, Coffey RT, Harris L, Wood B, Daniels MG, Bhattacharya T, Lapedes A, Polonis VR, McCutchan FE, Gilbert PB, Self SG, Korber BT, Montefiori DC, Mascola JR. 2010. Tiered Categorization of a Diverse Panel of HIV-1 Env Pseudoviruses for Assessment of Neutralizing Antibodies. J Virol 84:1439–1452.

64. deCamp A, Hraber P, Bailer RT, Seaman MS, Ochsenbauer C, Kappes J, Gottardo R, Edlefsen P, Self S, Tang H, Greene K, Gao H, Daniell X, Sarzotti-Kelsoe M, Gorny MK, Zolla-Pazner S, LaBranche CC, Mascola JR, Korber BT, Montefiori DC, Hahn BH. 2014. Global Panel of HIV-1 Env Reference Strains for Standardized Assessments of Vaccine-Elicited Neutralizing Antibodies. J Virol 88:2489–2507.

60. Seabold, Skipper, and Josef Perktold. "statsmodels: Econometric and statistical modeling with python." Proceedings of the 9th Python in Science Conference. 2010.

869 **Tables**

**Table 1 Biophysical properties of AMC011 and AMC016 trimers**

| | | | AMC011 SOSIP.v5.2 | | AMC016 SOSIP.v4.2 | |
|---|---|---|---|---|---|---|
| | | | parental | mutant | parental | mutant |
| Production [a] | | yield (mg/L) | 2.1 [+] | 1.0 | 2.0 | 1.5 |
| Thermostability | DSC | two State Model ($T_m$; °C) | 67 [+] | 64 [b] | 63 [b] | 63 [b] |
| Morphology | NS-EM | native-like trimers (%) | 100 [+] | 88 | 100 | 78 |
| Glycan composition | HILIC-UPLC | $Man_{5-9}$ (%) | 58.2 [+*] | 50.0 [*] | 53.4 [*] | 57.6 [*] |
| | | $Man_9$ (%) | 23.0 [+*] | 16.5 [*] | 23.9 [*] | 26.4 [*] |

[a]: Results were obtained from 293F cell-expressed and PGT145-purified SOSIP trimers

[b]: Results were obtained with D7324-tagged proteins

[*]: quantified w/o Endo H digestion

[+]: Schorcht et al., J. Virol, 2020 (3)

870

**Table 2 Cryo-EM parameters of the AMC016 and AMC018 trimers**

| | AMC018 SOSIP.v4.2 + PGV04 Fab | AMC016 SOSIP.v4.2 + PGV04 Fab |
|---|---|---|
| Microscope | FEI Titan Krios | FEI Titan Krios |
| Voltage, kV | 300 | 300 |
| Detector | Gatan K2 Sumit | Gatan K2 Sumit |
| Recording Mode | Counting | Counting |
| Magnification | 22.500 | 22.500 |
| Moive micrograph pixel size, Å | 1.31 | 1.31 |
| Dose rate, e-/[(camera pixel)*s] | 6.52 | 9.81 |
| No. of frames per moive micrograph | 35 | 35 |
| Frame exposure time, ms | 200 | 200 |
| Movie micrograph exposure time, s | 7 | 7 |
| Total dose, $e^-/Å^2$ | 26.6 | 40 |
| Defocus range, μm | -1.0 to -3.9 | -1.0 to -4.0 |
| No. of movie micrographs | 3916 | 3801 |
| No. of molecular projection images in map | 150333 | 77068 |
| Symmetry | C3 | C3 |
| Map resolution (FSC 0.143) | 3.49 | 4.10 |
| Map sharpening B-factor, $Å^2$ | -151.9 | -205.3 |
| No. of atoms in deposited model | 19623 | 20574 |
| MolProbity score | 0.95 | 0.72 |
| Clashscore | 0.41 | 0.67 |
| EMRinger score | 2.83 | 1.97 |
| Privateer | pass | pass |
| pdb-care | pass | pass |
| EMDB | EMDB-24675 | EMDB-24676 |
| PDB ID | 7RSN | 7RSO |

871

| Table 3 Tier categorization of the AMC016 and AMC018 viruses | | |
|---|---|---|
| | **$ID_{50}$ (dilution)** | |
| **Serum pool** | **AMC016** | **AMC018** |
| CHAVI-0406 pool | 10 | 10 |
| CHAVI-0060 pool | 20 | 49 |
| CHAVI-0642 pool | 10 | 22 |
| CHAVI-0293 pool | 22 | 118 |
| CHAVI-0598 pool | 23 | 125 |
| CHAVI-0585 pool | 90 | 288 |
| **GM $ID_{50}$** | **21** | **60** |

| | **$IC_{50}$ (µg/ml)** | |
|---|---|---|
| **Antibody** | **AMC016** | **AMC018** |
| VRC01 | 0.16 | 0.27 |
| 3BNC117 | 0.06 | 0.05 |
| CH31 | 0.25 | 0.11 |
| CH01 | >25 | >25 |
| PG9 | 3.9 | >5 |
| PG16 | 3.4 | >5 |
| 10-1074 | 0.08 | 0.06 |
| PGT128 | 0.16 | 0.04 |
| PGT121 | 0.14 | 0.13 |
| PGT151 | 0.02 | 0.02 |
| 2F5 | 11 | 4.7 |
| 4E10 | 24 | 8.5 |
| 10E8 | 2.2 | 0.9 |
| CH01-31 | 0.47 | 0.21 |
| **Classification** | **tier 2** | **tier 2** |

872

873 **Table legend**

874

875 **Table 3** The two subtype B viruses were tested against serum pools and a panel of bNAbs to
876 assess neutralization sensitivity. Upper part: Lack of neutralization at 1:20 is represented as a
877 value of 10. The reciprocal geometric mean (GM) $ID_{50}$ is the 50% inhibitory concentration.
878 The TZM-bl cell assays were performed at DUMC (see Material and Methods).

## Figure legends

**FIG 1** Characterization of the AMC016 SOSIP.v4.2 trimer. (A) NS-EM. (B) HILIC-UPLC analysis. Depicted in green are oligomannose/hybrid-type glycans and in magenta fully processed complex type glycans. (C) Site-specific glycan composition and occupancy using LC-MS on all 29 PNGS. The color code is the same as in panel B. The oligomannose/hybrid-type glycans are categorized according to the number of mannose residues and the presence or absence of fucose, respectively. Fully processed complex type glycans are arranged by the number of processed antenna and the presence of absence of fucose. The percentage of PNGS that are <90% occupied are indicated in grey.

**FIG 2** Characterization of the glycan mutant trimers AMC011 SOSIP.v5.2 Δ130Δ289 and AMC016 SOSIP.v4.2 Δ130Δ289. (A) Sequences of the AMC011 and AMC016 WT and glycan mutants (indicated as ΔΔ) at p130 and p289 (HXB2 nomenclature) in comparison to B41. (B) BN-PAGE analysis (left panel) and SDS-PAGE analyses (right panel) under reducing (+DTT) and non-reducing conditions (-DTT) The glycan mutant trimers are indicated as ΔΔ. (C) negative-stain EM analysis of the AMC011 Δ130Δ289 and AMC016 Δ130Δ289 trimers. (D) ELISA to compare the antigenicity of the parental and glycan mutant SOSIP trimers using a panel of bNAbs and non-neutralizing antibody 17b. (E) Glycan composition of the AMC011 Δ130Δ289 and AMC016 Δ130Δ289 trimers, analyzed by HILIC-UPLC. Green: oligomannose/hybrid-type glycans. Magenta: fully processed complex type glycans. See Table 1 for details.

**FIG 3** Site-specific glycan composition and occupancy of the AMC011 and AMC016 trimers from which N130 and N289 were deleted. (A) AMC011 SOSIP.v5.2 Δ130Δ289 and (B) AMC016 SOSIP.v4.2 Δ130Δ289 D7324-tagged. The data were obtained by LC-MS on all PNGS. The same color code is the same as used in Fig. 1.

**FIG 4** Percentage point difference in $Man_9$ content at each site. Differences were calculated at sites where $Man_9$ was resolved (% $Man_9$ mutant trimer - % $Man_9$ parental trimer) and indicated on the y-axis. The PNGS are listed on the x-axis. Yellow: AMC011 SOSIP Δ130Δ289. Lilac: AMC016 SOSIP Δ130Δ289 D7324-tagged. Glycan composition data on individual PNGS were obtained by LC-MS (for individual values see Fig. 3).

**FIG 5** Immunogenicity of rabbits immunized with the parental AMC011 and AMC016 trimers and the AMC011 Δ130Δ289 and AMC016 Δ130Δ289 trimer variants. (A) Immunization schedule. Rabbits were immunized at week 0, 4 and 20, indicated with black arrows. Sera from the week-22 bleed was analyzed (red arrow). The groups are indicated and color-coded according to the immunogen they received. B41 trimer-immunized animals from the same study were included for comparison (19). Statistically significant differences are indicated. The data was analyzed with a two-tailed Mann-Whitney *U* test. (B) Autologous neutralization titers ($ID_{50}$). (C) Relative neutralization of the AMC011 Δ289 and AMC016 Δ289 virus variants, based on the median $ID_{50}$ values. Autologous neutralization of the Δ130Δ289 virus variants was defined as 100% and the titers against the Δ289 variants compared to this benchmark. (D) Heterologous neutralization of the AMC011Δ289 and Δ130Δ289 viruses, the AMC016 Δ289 and Δ130Δ289 viruses and B41. (B), (C) and (D) The test viruses are indicated on the x-axis. (B) and (D) The median $ID_{50}$ per group is indicated by the horizontal black line, the dashed line represents the lower assay cut-off $ID_{50}$ value of 20. Week-22 serum from rabbit 2295 (AMC016 Δ130Δ289 trimer group) interfered with MLV infection, and was therefore excluded from further analysis. All individual $ID_{50}$ values can be found in Supplementary file 1.

**FIG 6** Cryo-EM structures of the AMC016 and AMC018 trimers. Molecular surface representation of (A) AMC016 SOSIP.v4.2 + PGV04 Fab and (B) AMC018 SOSIP.v4.2 + PGV04 Fab. (C) Structural overlays of AMC016 SOSIP.v4.2 and AMC018 SOSIP.v4.2 with BG505 SOSIP.664. (D) EM density maps for AMC016 SOSIP.v4.2 + PGV04 Fab and AMC018 SOSIP.v4.2 + PGV04 Fab with density corresponding to N-linked glycans in green. Data collection parameters are indicated in Table 2.

**FIG 7** Cryo-EM parameters used for the modelling of the AMC016 SOSIP.v4.2 and AMC018 SOSIP.v4.2 trimers, complexed with PGV04 Fab. (A) Fourier shell correlation curves calculated in cryoSPARC during final refinement. (B) Local resolution maps. Colors represent the resolution (3.0 Å to > 4.8 Å).

**FIG 8** Autologous neutralization of a panel of SOSIP trimers with different characteristics. (A) The autologous NAb response at week 22 of rabbits immunized with SOSIP trimers from subtype A, B and C. The trimers lack zero to four conserved PNGS. Grey spheres: SOSIP trimers with previously published immunogenicity (n≥5). Red squares: newly analyzed

SOSIP trimers of study C0048-15 and PA0064-16 (n=5; n=4 for the AMC016 group) (see Material and Methods for details) (2, 3, 27). The black line indicates the median $ID_{50}$, the dashed line represents the lower assay cutoff $ID_{50}$ value of 20. Listed are the tier categorization, genetic subtype, $T_m$ and the number of missing conserved PNGS. (B) Analysis of the overall glycan hole area, using the Glycan Shield Mapping tool (21). The color code used is the same as in panel A. (A) and (B) SOSIP trimers are ordered based on the median $ID_{50}$ values, from lowest to highest. Individual values are shown in Supplemental file 2.

**FIG 9** The size of the glycan hole area created by the absence of N130 and N289. The SOSIP trimers from Fig. 8 that lack one or both glycans, either naturally or via knock-out, were analyzed with the Glycan Shield Mapping tool (21). For some trimers the missing N130 glycan did not create a glycan hole. SOSIP trimers are ordered based on the median $ID_{50}$ values, from lowest to highest.

**FIG 10** Fitted correlation based on the mean regression coefficient of log glycan hole area and log autologous neutralization. Tier, subtype, $T_m$ and number of missing PNGS were not assumed to have any effect. (A) Data points are the median log autologous neutralization values for each trimer, across all animals. The linear regression coefficient (β) is indicated. (B) Coefficients of predictor variables in the generalized linear model.

A

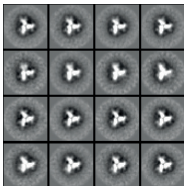

B

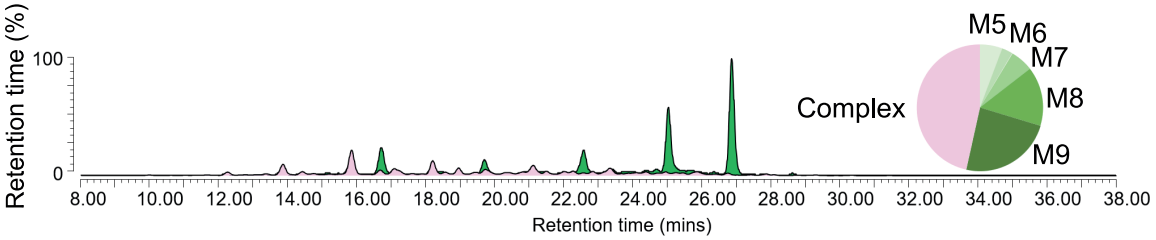


C

| | N88 | N130 | N134b | N136 | N142 | N156 | N160 | N188 | N197 | N230 | N234 | N241 | N262 | N276 | N289 | N295 | N301 | N332 | N339 | N356 | N386 | N392 | N398 | N411 | N448 | N462 | N611 | N616 | N625 | N637 |
|---|---|---|---|---|---|---|---|---|---|---|---|---|---|---|---|---|---|---|---|---|---|---|---|---|---|---|---|---|---|---|
| High Mannose | 44 | 67 | 72 | 15 | 17 | 97 | 100 | 67 | 89 | 100 | 83 | 70 | 100 | 98 | 50 | 100 | 87 | 100 | 100 | 56 | 100 | 100 | 99 | 99 | 100 | 30 | 16 | 10 | 23 | 77 |
| M9 | 0 | | | | | 61 | 32 | 0 | 28 | 88 | | | 80 | 1 | | | | 87 | 35 | 0 | 81 | 48 | 86 | | 77 | 0 | | | 0 | 13 |
| M8 | 0 | | | | | 25 | 47 | 6 | 23 | 12 | | | 18 | 43 | | | | 10 | 38 | 7 | 14 | 49 | 12 | | 15 | 2 | | | 2 | 16 |
| M7 | 1 | | | | | 4 | 12 | 12 | 16 | 0 | | | 2 | 26 | | | | 2 | 14 | 10 | 3 | 2 | 0 | | 4 | 5 | | | 6 | 22 |
| M6 | 3 | | | | | 3 | 5 | 10 | 9 | 0 | | | 0 | 12 | | | | 1 | 8 | 5 | 1 | 1 | 0 | | 2 | 3 | | | 1 | 1 |
| M5 | 36 | | | | | 2 | 4 | 22 | 12 | 0 | | | 0 | 13 | | | | 1 | 4 | 21 | 1 | 1 | 0 | | 2 | 16 | | | 7 | 19 |
| M4 | 0 | | | | | 1 | 0 | 1 | 1 | 0 | | | 0 | 1 | | | | 0 | 0 | 4 | 0 | 0 | 0 | | 0 | 1 | | | 0 | 0 |
| M3 | 0 | | | | | 0 | 0 | 0 | 0 | 0 | | | 0 | 0 | | | | 0 | 0 | 1 | 0 | 0 | 0 | | 0 | 0 | | | 0 | 0 |
| Hybrid | 3 | | | | | 0 | 0 | 11 | 1 | 0 | | | 0 | 1 | | | | 0 | 1 | 3 | 0 | 0 | 0 | | 0 | 1 | | | 3 | 4 |
| FHybrid | 1 | | | | | 0 | 0 | 4 | 1 | 0 | | | 0 | 0 | | | | 0 | 0 | 4 | 0 | 0 | 0 | | 0 | 2 | | | 4 | 1 |
| A1 | 12 | | | | | 0 | 0 | 4 | 0 | 0 | | | 0 | 1 | | | | 0 | 0 | 2 | 0 | 0 | 0 | | 0 | 1 | | | 4 | 3 |
| FA1 | 1 | | | | | 0 | 0 | 8 | 2 | 0 | | | 0 | 0 | | | | 0 | 0 | 12 | 0 | 0 | 0 | | 0 | 14 | | | 7 | 4 |
| A2/A1B | 24 | | | | | 0 | 0 | 1 | 0 | 0 | | | 0 | 0 | | | | 0 | 0 | 0 | 0 | 0 | 0 | | 0 | 0 | | | 6 | 0 |
| FA2/FA1B | 8 | 0 | 0 | 78 | 42 | 0 | 0 | 12 | 7 | 0 | 14 | 8 | 0 | 1 | 2 | 0 | 0 | 0 | 0 | 16 | 0 | 0 | 0 | 0 | 0 | 28 | 22 | 7 | 35 | 8 |
| A3/A2B | 4 | | | | | 0 | 0 | 0 | 0 | 0 | | | 0 | 0 | | | | 0 | 0 | 0 | 0 | 0 | 0 | | 0 | 0 | | | 2 | 0 |
| FA3/FA2B | 7 | | | | | 0 | 0 | 3 | 2 | 0 | | | 0 | 0 | | | | 0 | 0 | 13 | 0 | 0 | 0 | | 0 | 25 | | | 19 | 3 |
| A4/A3B | 0 | | | | | 0 | 0 | 0 | 0 | 0 | | | 0 | 0 | | | | 0 | 0 | 0 | 0 | 0 | 0 | | 0 | 0 | | | 0 | 0 |
| FA4/FA3B | 0 | | | | | 0 | 0 | 0 | 0 | 0 | | | 0 | 0 | | | | 0 | 0 | 1 | 0 | 0 | 0 | | 0 | 2 | | | 1 | 0 |
| Occupancy | 100 | 67 | 72 | 93 | 58 | 97 | 100 | 96 | 100 | 100 | 97 | 79 | 100 | 100 | 52 | 100 | 87 | 100 | 100 | 99 | 100 | 100 | 99 | 99 | 100 | 100 | 37 | 17 | 97 | 95 |

**FIG 1**

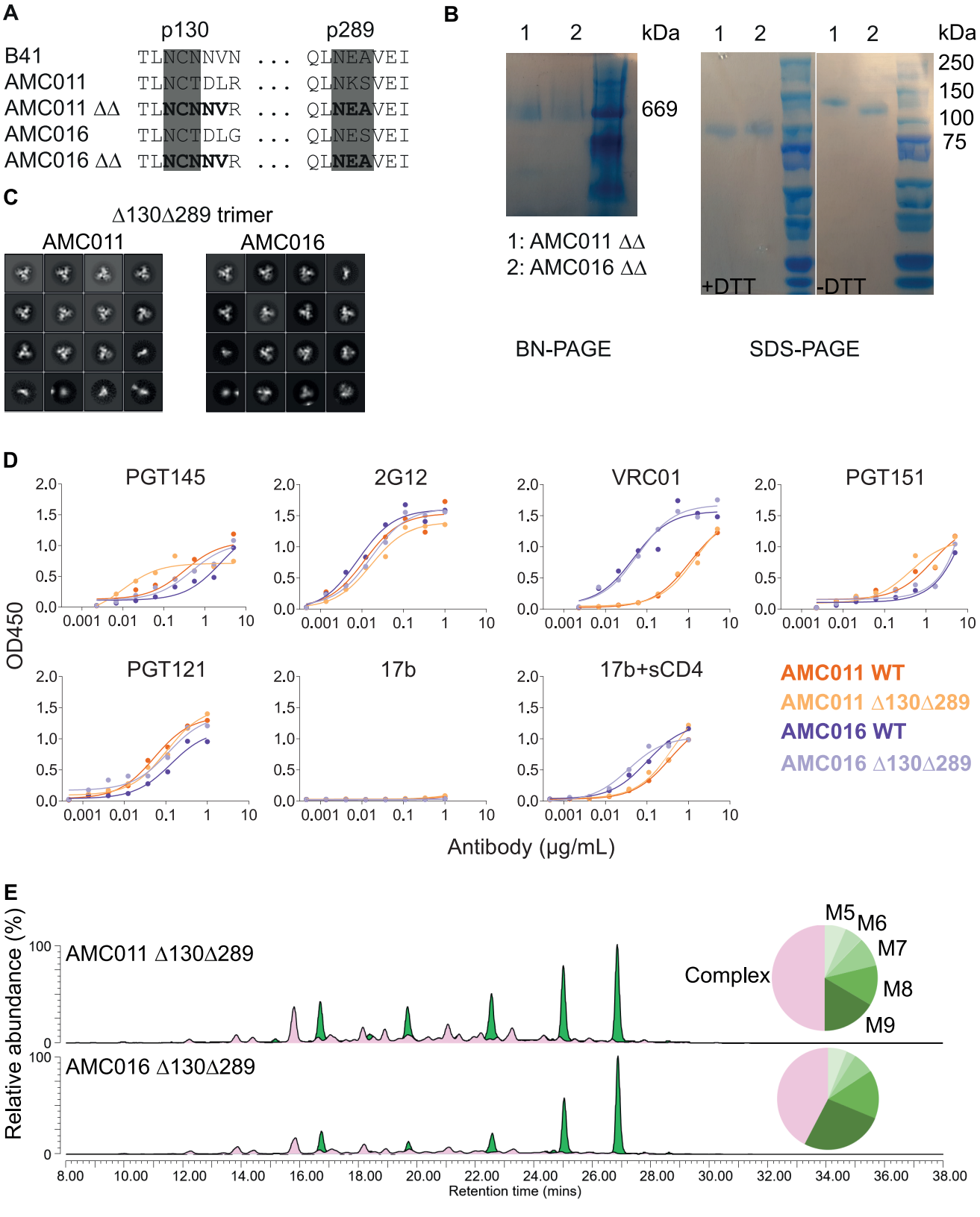


**FIG 2**

**A** AMC011 Δ130Δ289

| | N88 | N130 | N136 | N141 | N141c | N156 | N160 | N188 | N197 | N234 | N241 | N262 | N276 | N289 | N295 | N301 | N332 | N339 | N355 | N362 | N386 | N392 | N396 | N406 | N448 | N461 | N611 | N616 | N625 | N637 |
|---|---|---|---|---|---|---|---|---|---|---|---|---|---|---|---|---|---|---|---|---|---|---|---|---|---|---|---|---|---|---|
| High Mannose | 7 | | 79 | 10 | 31 | 93 | 66 | 45 | 61 | 98 | 88 | 93 | 98 | | 100 | 95 | 100 | 98 | 1 | 97 | 100 | 100 | 100 | 100 | 100 | 6 | 0 | 1 | 4 | 34 |
| M9 | 0 | | | | | 20 | 19 | 0 | 11 | | | 81 | 8 | | | | 79 | 2 | 0 | 78 | 75 | | | 0 | 55 | 0 | | | 0 | 1 |
| M8 | 0 | | | | | 39 | 36 | 1 | 22 | | | 11 | 44 | | | | 20 | 6 | 0 | 18 | 25 | | | 26 | 27 | 0 | | | 0 | 3 |
| M7 | 0 | | | | | 14 | 5 | 4 | 11 | | | 1 | 29 | | | | 1 | 60 | 0 | 1 | 0 | | | 48 | 12 | 0 | | | 0 | 6 |
| M6 | 0 | | | | | 5 | 0 | 2 | 7 | | | 0 | 8 | | | | 0 | 19 | 0 | 0 | 0 | | | 27 | 5 | 0 | | | 0 | 6 |
| M5 | 4 | | | | | 10 | 3 | 19 | 5 | | | 0 | 3 | | | | 0 | 8 | 0 | 0 | 0 | | | 0 | 1 | 3 | | | 1 | 10 |
| M4 | 0 | | | | | 0 | 2 | 0 | 0 | | | 0 | 1 | | | | 0 | 0 | 0 | 0 | 0 | | | 0 | 0 | 0 | | | 0 | 0 |
| M3 | 0 | | | | | 0 | 0 | 0 | 0 | | | 0 | 0 | | | | 0 | 0 | 0 | 0 | 0 | | | 0 | 0 | 0 | | | 0 | 0 |
| Hybrid | 1 | | | | | 1 | 2 | 9 | 2 | | | 0 | 7 | | | | 0 | 2 | 0 | 0 | 0 | | | 0 | 0 | 1 | | | 2 | 5 |
| FHybrid | 2 | | | | | 2 | 0 | 10 | 2 | | | 0 | 0 | | | | 0 | 0 | 1 | 0 | 0 | | | 0 | 0 | 1 | | | 1 | 2 |
| A1 | 3 | | | | | 0 | 1 | 2 | 1 | | | 0 | 1 | | | | 0 | 0 | 0 | 0 | 0 | | | 0 | 0 | 1 | | | 2 | 3 |
| FA1 | 3 | | | | | 3 | 1 | 15 | 5 | | | 0 | 0 | | | | 0 | 0 | 4 | 0 | 0 | | | 0 | 0 | 7 | | | 2 | 4 |
| A2/A1B | 16 | | | | | 0 | 3 | 0 | 0 | | | 0 | 1 | | | | 0 | 0 | 0 | 0 | 0 | | | 0 | 0 | 0 | | | 11 | 0 |
| FA2/FA1B | 16 | | | | | 3 | 17 | 28 | 23 | | | 0 | 0 | | | | 0 | 0 | 70 | 0 | 0 | | | 0 | 0 | 32 | | | 49 | 30 |
| A3/A2B | 17 | | | | | 0 | 1 | 0 | 0 | | | 0 | 0 | | | | 0 | 0 | 0 | 0 | 0 | | | 0 | 0 | 0 | | | 3 | 0 |
| FA3/FA2B | 32 | | | | | 0 | 10 | 9 | 9 | | | 7 | 0 | | | | 0 | 0 | 21 | 0 | 0 | | | 0 | 0 | 50 | | | 27 | 6 |
| A4/A3B | 0 | | | | | 0 | 0 | 0 | 0 | | | 0 | 0 | | | | 0 | 0 | 0 | 0 | 0 | | | 0 | 0 | 0 | | | 0 | 0 |
| FA4/FA3B | 4 | | | | | 0 | 0 | 1 | 1 | | | 0 | 0 | | | | 0 | 2 | 3 | 0 | 0 | | | 0 | 0 | 5 | | | 2 | 0 |
| Occupancy | 100 | | 79 | 80 | 100 | 100 | 100 | 100 | 100 | 99 | 97 | 100 | 100 | | 100 | 100 | 100 | 100 | 100 | 97 | 100 | 100 | 100 | 100 | 100 | 99 | 60 | 1 | 100 | 78 |

**B** AMC016 Δ130Δ289

| | N88 | N130 | N134b | N136 | N142 | N156 | N160 | N188 | N197 | N230 | N234 | N241 | N262 | N276 | N289 | N295 | N301 | N332 | N339 | N356 | N386 | N392 | N398 | N411 | N448 | N462 | N611 | N616 | N625 | N637 |
|---|---|---|---|---|---|---|---|---|---|---|---|---|---|---|---|---|---|---|---|---|---|---|---|---|---|---|---|---|---|---|
| High Mannose | 68 | | 90 | 63 | 58 | 96 | 100 | 53 | 67 | 100 | 100 | 99 | 100 | 98 | | 100 | 100 | 100 | 95 | 33 | 100 | 100 | 100 | 100 | 100 | 38 | 18 | 22 | 56 | 68 |
| M9 | 0 | | 0 | | | 29 | 5 | 0 | 9 | 83 | | | 91 | 1 | | | | 92 | 3 | 0 | 78 | | | 83 | 89 | 0 | | | 0 | 6 |
| M8 | 4 | | 32 | | | 44 | 70 | 11 | 11 | 17 | | | 9 | 57 | | | | 7 | 46 | 4 | 22 | | | 15 | 9 | 6 | | | 8 | 21 |
| M7 | 6 | | 18 | | | 10 | 13 | 13 | 22 | 0 | | | 0 | 23 | | | | 1 | 24 | 4 | 0 | | | 2 | 1 | 9 | | | 10 | 16 |
| M6 | 12 | | 12 | | | 4 | 5 | 7 | 8 | 0 | | | 0 | 8 | | | | 0 | 9 | 3 | 0 | | | 0 | 0 | 4 | | | 12 | 6 |
| M5 | 39 | | 23 | | | 5 | 6 | 10 | 12 | 0 | | | 0 | 3 | | | | 0 | 5 | 10 | 0 | | | 0 | 0 | 15 | | | 10 | 11 |
| M4 | 0 | | 0 | | | 3 | 0 | 0 | 0 | 0 | | | 0 | 1 | | | | 0 | 0 | 3 | 0 | | | 0 | 0 | 0 | | | 0 | 0 |
| M3 | 0 | | 0 | | | 1 | 0 | 0 | 0 | 0 | | | 0 | 0 | | | | 0 | 0 | 1 | 0 | | | 0 | 0 | 0 | | | 0 | 0 |
| Hybrid | 6 | | 1 | | | 0 | 1 | 4 | 2 | 0 | | | 0 | 3 | | | | 0 | 7 | 2 | 0 | | | 0 | 0 | 1 | | | 5 | 3 |
| FHybrid | 2 | | 3 | | | 1 | 0 | 7 | 2 | 0 | | | 0 | 0 | | | | 0 | 0 | 6 | 0 | | | 0 | 0 | 2 | | | 10 | 4 |
| A1 | 4 | | 0 | | | 0 | 0 | 1 | 1 | 0 | | | 0 | 0 | | | | 0 | 0 | 1 | 0 | | | 0 | 0 | 1 | | | 2 | 1 |
| FA1 | 3 | | 4 | | | 1 | 0 | 7 | 3 | 0 | | | 0 | 0 | | | | 0 | 0 | 9 | 0 | | | 0 | 0 | 5 | | | 5 | 3 |
| A2/A1B | 12 | | 0 | | | 0 | 0 | 0 | 0 | 0 | | | 0 | 1 | | | | 0 | 0 | 0 | 0 | | | 0 | 0 | 2 | | | 2 | 0 |
| FA2/FA1B | 8 | | 2 | | | 1 | 0 | 23 | 20 | 0 | | | 0 | 1 | | | | 0 | 0 | 23 | 0 | | | 0 | 0 | 24 | | | 25 | 16 |
| A3/A2B | 2 | | 0 | | | 0 | 0 | 0 | 0 | 0 | | | 0 | 0 | | | | 0 | 0 | 0 | 0 | | | 0 | 0 | 0 | | | 0 | 0 |
| FA3/FA2B | 3 | | 4 | | | 1 | 0 | 13 | 8 | 0 | | | 0 | 0 | | | | 0 | 0 | 31 | 0 | | | 0 | 0 | 27 | | | 10 | 8 |
| A4/A3B | 0 | | 0 | | | 0 | 0 | 0 | 0 | 0 | | | 0 | 0 | | | | 0 | 0 | 0 | 0 | | | 0 | 0 | 0 | | | 0 | 0 |
| FA4/FA3B | 0 | | 1 | | | 0 | 0 | 2 | 1 | 0 | | | 0 | 0 | | | | 0 | 5 | 2 | 0 | | | 0 | 0 | 3 | | | 0 | 0 |
| Occupancy | 100 | | 100 | 99 | 59 | 100 | 100 | 100 | 100 | 100 | 100 | 99 | 100 | 100 | | 100 | 100 | 100 | 100 | 100 | 100 | 100 | 100 | 100 | 100 | 100 | 29 | 22 | 100 | 96 |

**FIG 3**

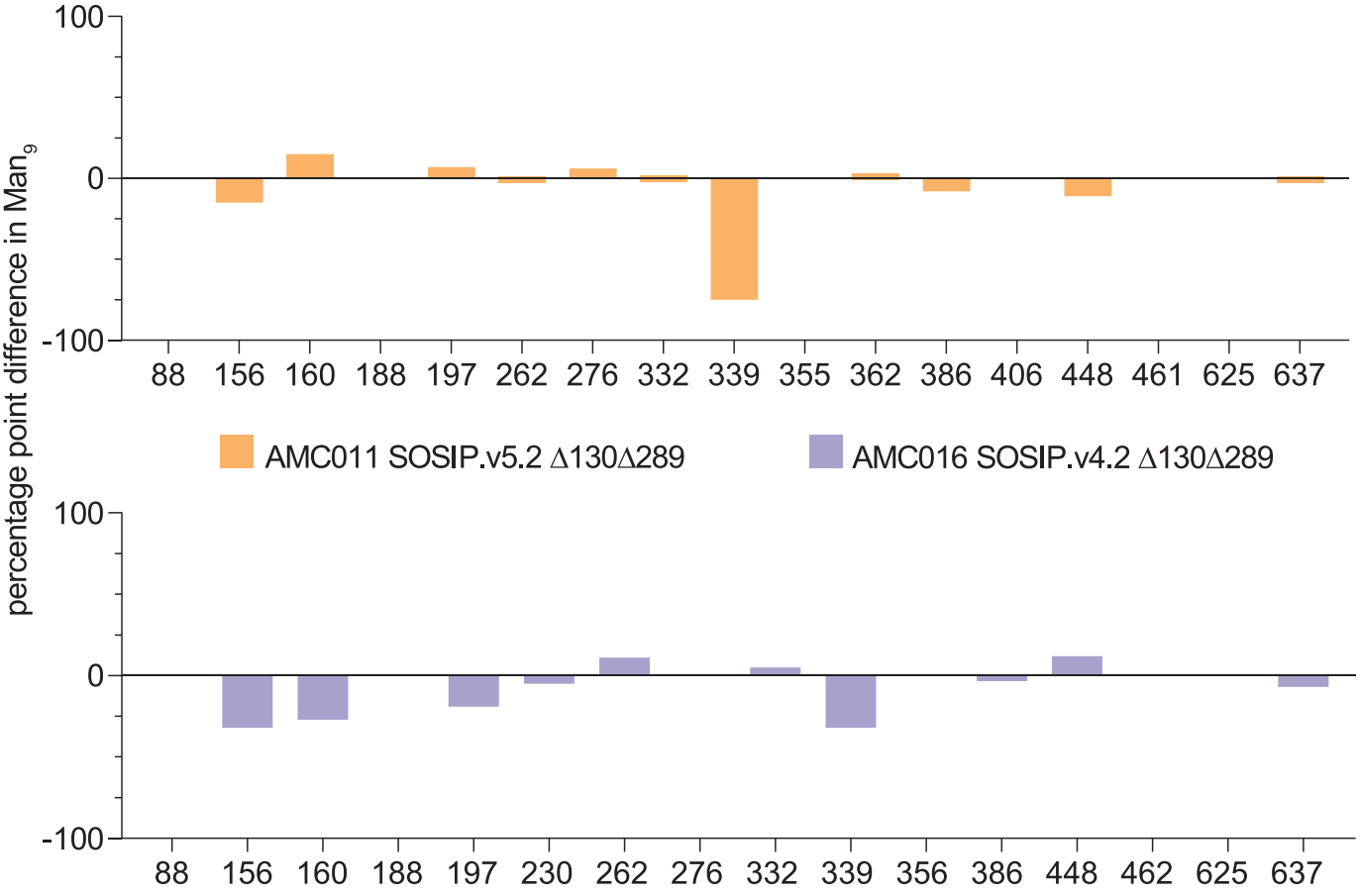


**FIG 4**

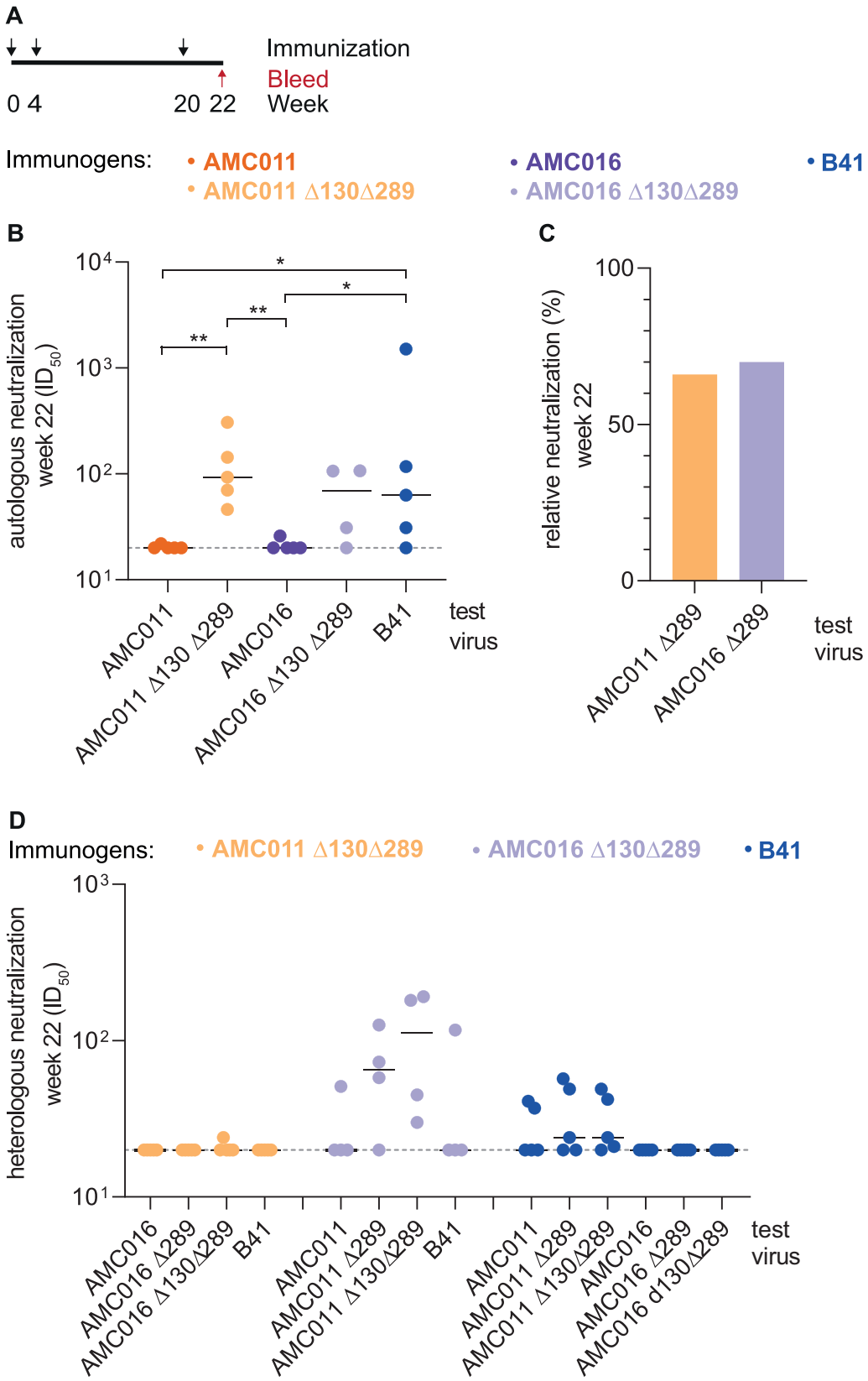


**FIG 5**

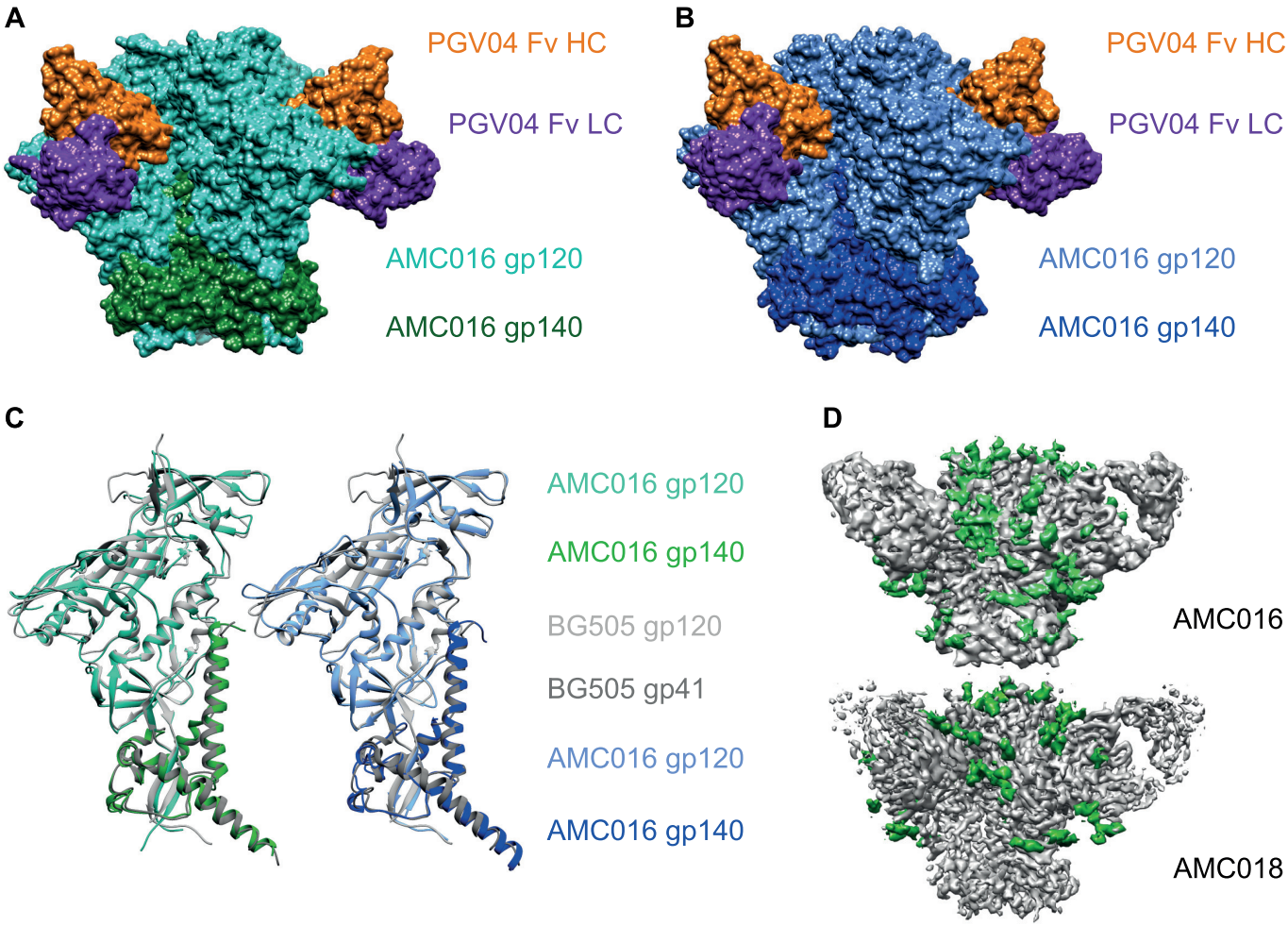


**FIG 6**

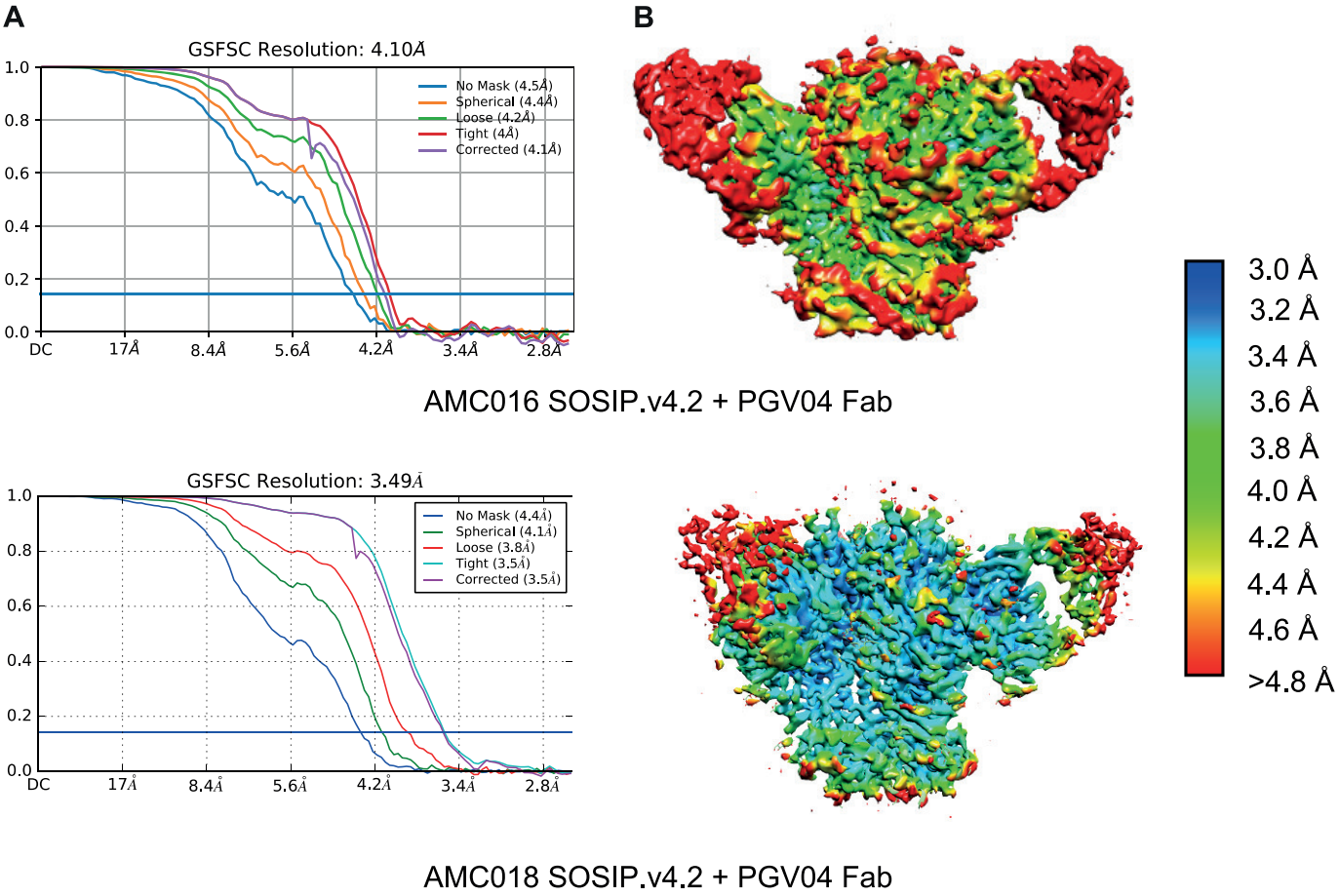


**FIG 7**

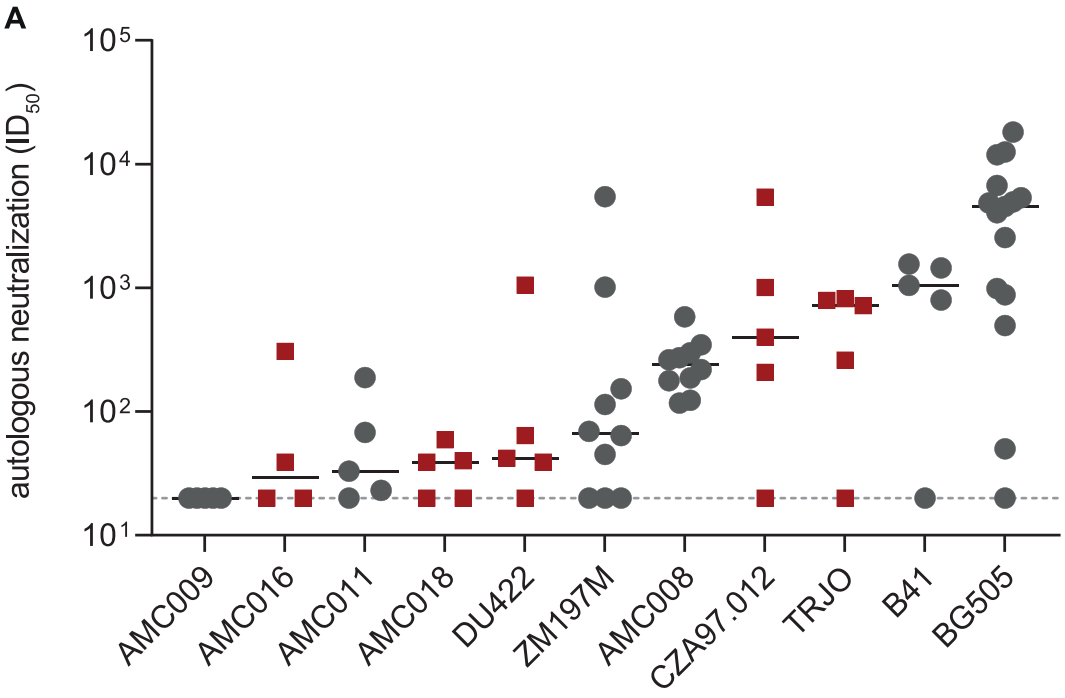


| | | | | | | | | | | | |
|---|---|---|---|---|---|---|---|---|---|---|---|
| tier | 2 | 2 | 2 | 2 | 2 | 1B | 1B | 2 | 2 | 2 | 2 |
| subtype | B | B | B | B | C | C | B | C | B | B | A |
| $T_m$ (°C) | 68 | 63 | 63 | 62 | 63 | 66 | 64 | 69 | 70 | 62 | 72 |
| # missing PNGS | 0 | 0 | 0 | 1 | 1 | 1 | 1 | 4 | 0 | 2 | 3 |

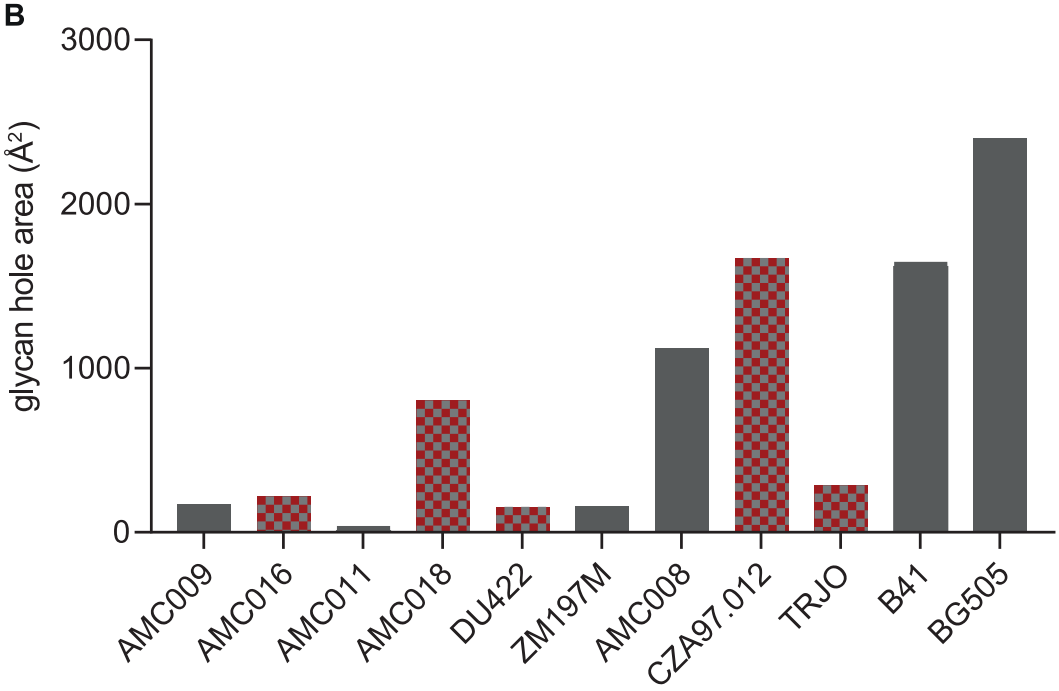


**FIG 8**

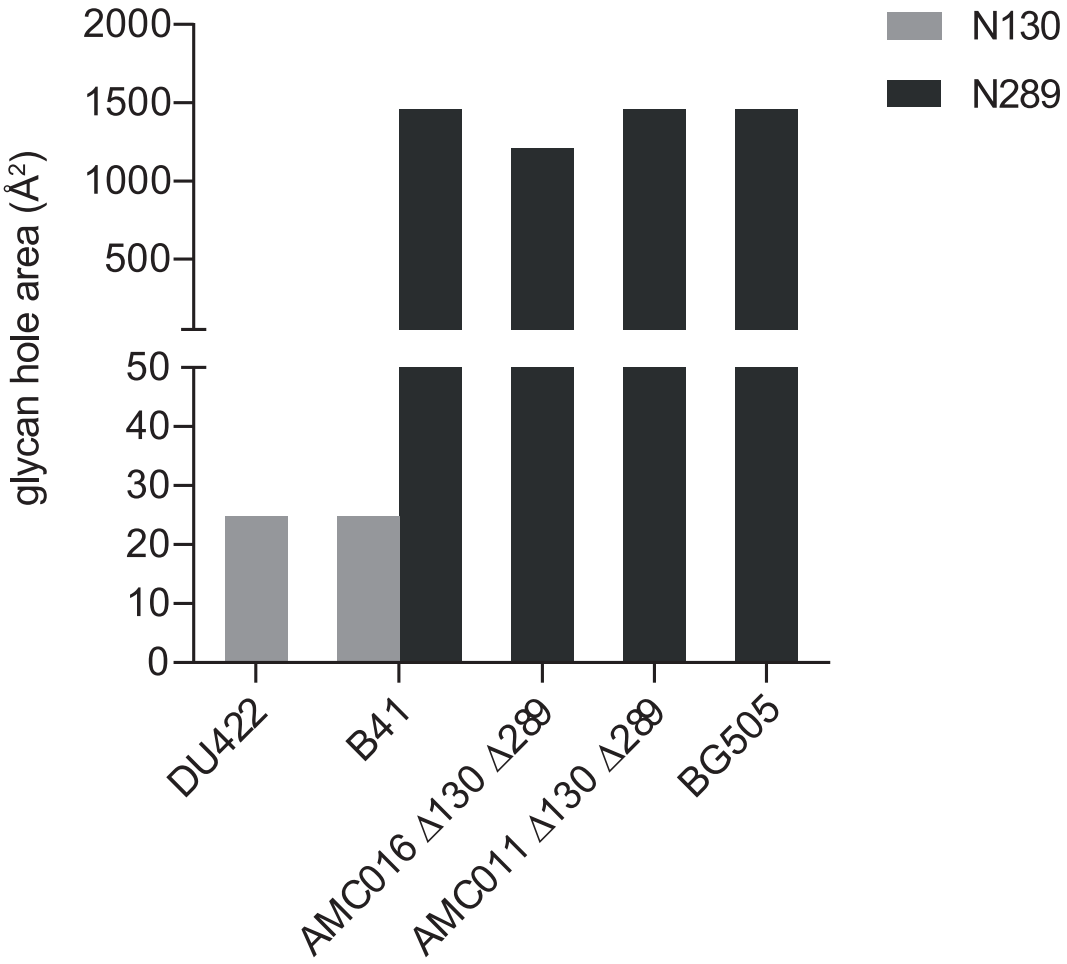


**FIG 9**

A

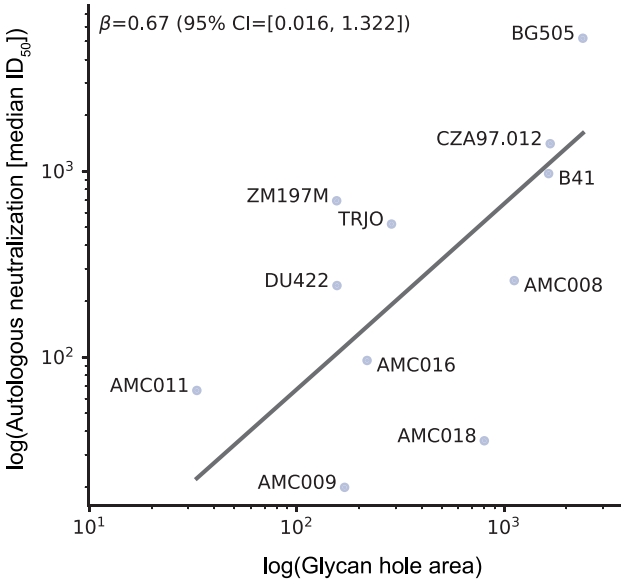


FIG 10

B

| Variable | Mean regression coefficient (β) | Standard Error | p-value | 95% confidence interval | |
|---|---|---|---|---|---|
| | | | | Lower | Upper |
| Tier | -0.299 | 0.363 | 0.41 | -1.010 | 0.412 |
| Subtype | 0.143 | 0.261 | 0.583 | -0.369 | 0.656 |
| $T_m$ | 0.316 | 0.328 | 0.336 | -0.327 | 0.959 |
| Number of missing PNGS | 0.28 | 0.105 | 0.205 | -0.136 | 0.63 |
| **Log (Glycan hole area)** | **0.669** | **0.333** | **0.045** | **0.016** | **1.322** |